Clim Dyn (2016) 47:3737–3765
DOI 10.1007/s00382-016-3039-1

The impact of eastern equatorial Pacific convection on the diversity of boreal winter El Niño teleconnection patterns

Nathaniel C. Johnson[1,2,3] · **Yu Kosaka**[2,4]

Received: 17 August 2015 / Accepted: 11 February 2016 / Published online: 27 February 2016

Abstract It is widely recognized that no two El Niño episodes are the same; hence the predictable variations of the climate impacts associated with El Niño remain an open problem. Through an analysis of observational data and of large ensembles from six climate models forced by the observed time-varying sea surface temperatures (SSTs), this study raises the argument that the most fundamental predictable variations of boreal wintertime El Niño teleconnection patterns relate to the distinction between convective (EPC) and non-convective eastern Pacific (EPN) events. This distinction is a consequence of the nonlinear relationship between deep convection and eastern Pacific SSTs, and the transition to a convective eastern Pacific has a predictable relationship with local and tropical mean SSTs. Notable differences (EPC minus EPN) between the teleconnection patterns include positive precipitation differences over southern North America and northern Europe, positive temperature differences over northeast North America, and negative temperature differences over the Arctic. These differences are stronger and more statistically significant than the more common partitioning between eastern Pacific and central Pacific El Niño. Most of the seasonal mean composite anomalies associated with EPN El Niño are not statistically significant owing to the weak SST forcing and small sample sizes; however, the EPN teleconnection is more robust on subseasonal timescales following periods when the EPN pattern of tropical convection is active. These findings suggest that the differences between EPC and EPN climate impacts are physically robust and potentially useful for intraseasonal forecasts for lead times of up to a few weeks.

Keywords El Niño · Teleconnection patterns · Pacific/North American pattern · Convective threshold · Eastern Pacific · Subseasonal-to-seasonal climate prediction · Arctic amplification

1 Introduction

The El Niño-Southern Oscillation (ENSO) is the dominant mode of tropical atmosphere–ocean interaction on interannual timescales and the primary source of seasonal predictability over a large fraction of the globe. This source of predictability takes root in the convective excitation of large-scale atmospheric teleconnection patterns that are characterized by significant remote weather and climate impacts (Horel and Wallace 1981; Ropelewski and Halpert 1987; Kiladis and Diaz 1989; Halpert and Ropelewski 1992; Trenberth et al. 1998; Trenberth and Caron 2000; Trenberth and Smith 2009; Chiodi and Harrison 2015; L'Heureux et al. 2015). Of particular interest for long-range forecasting, these teleconnection patterns, which are most prominent in the upper tropospheric geopotential height and streamfunction fields, significantly modify surface temperature and precipitation patterns. Both ENSO variability and the associated teleconnections tend to be strongest in

✉ Nathaniel C. Johnson
Nathaniel.Johnson@noaa.gov

[1] International Pacific Research Center, SOEST, University of Hawaii at Manoa, Honolulu, HI, USA

[2] Scripps Institution of Oceanography, University of California, San Diego, La Jolla, CA, USA

[3] Cooperative Institute for Climate Science, Princeton University, NOAA GFDL 201 Forrestal Rd., Princeton, NJ 08540, USA

[4] Research Center for Advanced Science and Technology, University of Tokyo, Tokyo, Japan

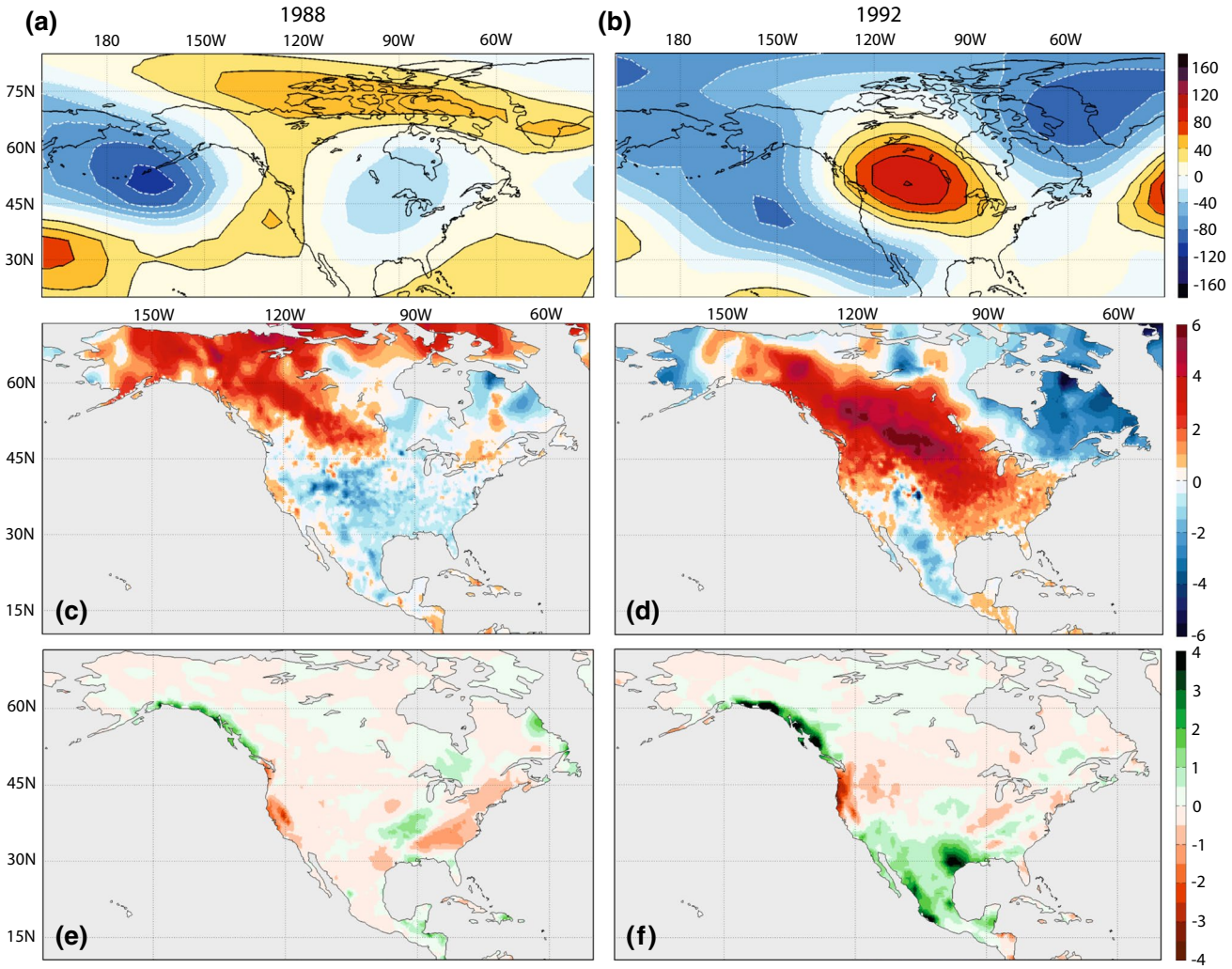

Fig. 1 December–March anomalies for two different El Niño episodes, (*left*) the 1988 event and (*right*) the 1992 event. **a**, **b** 300 hPa geopotential height anomalies (m), **c**, **d** T2m (°C), and **e**, **f** precipitation (mm d^{-1})

boreal winter, but the anomalies of temperature and precipitation persist into the warm season in some regions, particularly where land–atmosphere interactions reinforce soil moisture-related anomalies (Schubert et al. 2004; Hoerling et al. 2013). The prospects of ENSO-related seasonal predictability tend to focus on North America, the region immediately downstream of the ENSO-related tropical convection anomalies, but recently there has been an increased focus on the impact of ENSO on European climate (see Brönnimann 2007 and the references therein). This recent focus signifies renewed hope that the seasonal predictability associated with ENSO extends beyond the conventional influence regions, although the robustness and physical mechanisms of the more remote European link continue to be an active area of research and debate.

ENSO typically is monitored by sea surface temperatures (SSTs) in the equatorial eastern Pacific region, most notably in the so-called Niño 3.4 region (Barnston et al. 1997; Trenberth 1997), which extends from 5°S to 5°N and from 120°W to 170°W. Specifically, the National Oceanic and Atmospheric Administration (NOAA) defines an El Niño (La Niña) episode when the 3-month running mean Niño 3.4 SST anomaly is >0.5 °C (<−0.5 °C) for at least five consecutive overlapping, 3-month seasons. All other periods are classified as neutral ENSO. Although the robustness of the aforementioned ENSO teleconnections imply statistically significant composite climate anomalies associated with El Niño and La Niña across a large fraction of the globe, there is substantial inter-event variability for both phases of ENSO. To illustrate this point, Fig. 1 presents the boreal winter (December–March) 300 hPa geopotential height, two-meter air temperature (T2m), and precipitation anomalies for two El Niño episodes, the 1987/1988 and 1991/1992 events (additional descriptions

of the data and the two events are presented in Sects. 2, 3). Clearly, the climate anomalies associated with these two episodes are quite distinct, with oppositely signed anomalies in each field over large portions of North America.

Why do the climate anomalies vary so much among El Niño episodes and how much of this variability is predictable on seasonal timescales? We first must recognize that a large fraction of the seasonal variance among El Niño episodes is likely unpredictable owing to atmospheric internal variability (Hoerling and Kumar 1997; Kumar and Hoerling 1997; Sardeshmukh et al. 2000). Although the timescales of processes internal to the atmosphere are short, generally on the order of 10 days or less, such random weather variations still leave a substantial imprint on seasonal climate anomalies, dominating the tropical SST-induced variability over most regions (e.g., Sardeshmukh et al. 2000).

Despite this sober realization, hope remains that there exists variability in response among El Niño episodes that is predictable on seasonal timescales and that has not yet been fully exploited. Given that the location of maximum SST anomalies varies rather continuously among El Niño episodes (Giese and Ray 2011; Ray and Giese 2012; Johnson 2013), and that large-scale atmospheric teleconnection patterns are sensitive to the location of the tropical SST anomalies (Palmer and Mansfield 1986b; Barsugli and Sardeshmukh 2002), one may expect that the impacts of El Niño may depend on the particular "flavor" of El Niño (Trenbeth and Stepaniak 2001), as defined by the particular pattern of tropical SST anomalies. In particular, there has been considerable recent focus on two distinct types of El Niño. The canonical "Eastern Pacific" (EP) El Niño is the traditional form, featuring SST anomalies that peak in the eastern equatorial Pacific Ocean. The more recently highlighted "Central Pacific" (CP) El Niño (Yu and Kao 2007; Kao and Yu 2009), also referred as the "dateline El Niño" (Larkin and Harrison 2005), "El Niño Modoki" (Ashok et al. 2007), and "warm pool El Niño" (Kug et al. 2009), features positive equatorial SST anomalies centered near the International Date Line. Quite a few recent studies indicate that these two types of El Niño have distinct global impacts (Larkin and Harrison 2005; Weng et al. 2007; Ashok et al. 2007; Mo 2010; Hu et al. 2012; Yu et al. 2012; Yu and Zou 2013), suggesting that such variations are potentially predictable on seasonal timescales.

Attempts to distinguish these two types of El Niño, however, raise several challenges. First, as mentioned above, the location of maximum SST anomalies varies rather continuously among El Niño episodes and therefore does not follow a clear bimodal distribution, thereby igniting a debate about whether two distinct El Niño modes truly exist (Giese and Ray 2011; Ray and Giese 2012; Johnson 2013; Capotondi et al. 2015). Second, this lack of bimodality leads to arbitrariness and variations in how EP and CP El Niño events are defined, and the distinctions between the teleconnection patterns are quite sensitive to the precise choice of definitions (Garfinkel et al. 2013), possibly resulting in conflicting reports on the impacts of EP versus CP El Niño. For example, Graf and Zanchettin (2012) suggest that the CP El Niño is associated with the negative phase of the North Atlantic Oscillation (NAO), whereas Sung et al. (2014) counter that the EP El Niño is associated with the negative phase of NAO; the source of this disparity is not immediately evident.

Chiodi and Harrison (2013) recently proposed another perspective, suggesting that the key factor modulating the impacts of El Niño over the U.S. and many other regions of the globe (Chiodi and Harrison 2015) is the presence or absence of deep convection in the eastern equatorial Pacific Ocean. They further suggest that only those El Niño episodes that induce deep convection [i.e., negative outgoing longwave radiation (OLR) anomalies] in the eastern equatorial Pacific, which they term "OLR- El Niño events", are associated with robust U.S. climate impacts. As argued further in the remainder of this study, this distinction between "OLR" and "non-OLR" El Niño events likely relates to the nonlinear relationship between deep convection and eastern equatorial Pacific SSTs. This nonlinearity and its potential implications for ENSO teleconnections have been noted in previous studies (Hoerling et al. 1997, 2001; Hannachi 2001; Kumar et al. 2005; Peng and Kumar 2005; Toniazzo and Scaife 2006; Frauen et al. 2014), but these studies do not provide a thorough treatment of how the presence or absence of eastern Pacific deep convection relates to the diversity of El Niño teleconnection patterns and to the myriad recent studies focused on this topic.

Additional studies suggest other factors that may modulate El Niño teleconnection patterns, including interdecadal oscillations (Gershunov and Barnett 1998; DeWeaver and Nigam 2002) and the quasi-biennial oscillation (QBO) (Garfinkel and Hartmann 2008, 2010), but a review of these ideas is beyond the scope of this study. The variety of proposed hypotheses, however, does suggest that there is a need to clarify the most fundamental factors responsible for predictable variations in El Niño teleconnection patterns and their associated remote impacts. In this study, we follow the spirit of Chiodi and Harrison (2013, 2015) by arguing that one of the most fundamental modulators of Northern Hemisphere, boreal winter El Niño teleconnections is the presence or absence of deep convection in the eastern equatorial Pacific Ocean, which is more fundamental than the distinction between the EP or CP type of El Niño. Unlike Chiodi and Harrison (2013), however, we further argue that the non-convective eastern Pacific El Niño is clearly distinguishable by the eastern equatorial Pacific and tropical mean SSTs, as the distinction is a reflection of the nonlinear relationship between SST and deep convection

in the eastern Pacific cold tongue region. We examine differences in the seasonal climate impacts between these two types of El Niño, focusing on Pacific/North America region but also including some discussion of European impacts, given the recent focus on possible predictability associated with ENSO over Europe. We also examine the intraseasonal evolution of the El Niño teleconnection patterns and associated climate impacts, and we propose some mechanisms that may contribute to the differences between these teleconnection patterns.

The remainder of this article is organized as follows. Section 2 presents the observational, reanalysis, and climate model data and analysis methods used in this study. Section 3 describes the morphology of convective and non-convective eastern Pacific El Niño episodes, including the seasonal and intraseasonal composite analysis. Section 4 provides some analysis and discussion of dynamical mechanisms contributing to the contrast in the teleconnection patterns. The article follows with a discussion in Sect. 5 and summary in Sect. 6.

2 Materials and methods

In this study we make extensive use of composite analysis to document the differences between convective eastern Pacific (EPC) and non-convective eastern Pacific (EPN) El Niño episodes. Here we describe the various sources of observational, reanalysis, and climate model simulations forced by the time-varying SSTs.

2.1 Reanalysis and observational data sets

We focus on 21 El Niño episodes from 1950 to 2013 (see Table 1 for the list of events) using the Niño 3.4 SST definition discussed in the introduction. We analyze the tropical SST patterns and their relationship with deep convection with monthly mean, December–March SST data from Extended Reconstructed Sea Surface Temperature Dataset, Version 3b (ERSST v3b; Xue et al. 2003; Smith et al. 2008), which is on a 2° latitude-longitude grid. We also analyze both daily and monthly tropical OLR data, which serve as a proxy for deep convection, obtained from the National Oceanic and Atmospheric Administration (Liebmann and Smith 1996). These satellite-derived data, which are on a 2.5° latitude-longitude grid, are analyzed for the period from 1979 to 2012. Therefore, the analysis of tropical SST-deep convection relationships is limited to the more recent time period of satellite coverage. For this analysis, the tropical OLR and SST are linearly interpolated to a common grid with 2.5° spatial resolution.

To provide an understanding for the nonlinear relationship between deep convection and SSTs in the equatorial eastern Pacific region, we briefly examine the relationship between climatological SSTs and mean conditional instability. For this analysis, we calculated the climatological SSTs and mean saturation equivalent potential temperature, θ_{es}, defined as

$$\theta_{es} = \theta \exp\left(\frac{L_c q_s}{c_p T}\right), \tag{1}$$

where θ is the potential temperature, L_c is the latent heat of condensation, q_s is the saturation mixing ratio, c_p is the specific heat of dry air at constant pressure, and T is the temperature. We calculated θ_{es} in the deep tropics from 20°S to 20°N with monthly mean fields of temperature at 23 pressure levels between 200 and 1000 hPa, provided by the European Center for Medium-Range Weather Forecasts ERA-Interim reanalysis (Dee et al. 2011), for the period of 1979–2013.

Table 1 List of the 21 El Niño episodes considered in this study

El Niño years	Detrended Niño 3.4 SST (°C)	EP or CP	EP RSST (°C)
1951–1952	0.32	EP	0.18
1953–1954	0.41	CP	0.39
1957–1958	1.57	CP	**1.32**
1958–1959	0.47	CP	0.28
1963–1964	0.65	CP	0.46
1965–1966	1.19	CP	**1.07**
1968–1969	0.99	CP	0.58
1969–1970	0.45	EP	0.13
1972–1973	1.49	EP	**1.15**
1976–1977	0.55	EP	0.51
1977–1978	0.52	CP	0.39
1982–1983	2.07	EP	**1.86**
1986–1987	1.24	EP	**1.03**
1987–1988	0.63	CP	0.14
1991–1992	1.66	CP	**1.47**
1994–1995	1.05	CP	0.63
1997–1998	2.05	EP	**1.48**
2002–2003	1.01	CP	0.49
2004–2005	0.59	CP	0.08
2006–2007	0.57	EP	0.08
2009–2010	1.48	CP	**0.88**

The first column indicates the years of the DJFM season. The second column provides the linearly detrended DJFM Niño 3.4 SST. The third column indicates the El Niño category, Eastern Pacific (EP) or Central Pacific (CP), according to the consensus categorization of Yu et al. (2012). The fourth column indicates the DJFM RSST in the eastern Pacific box from 5°S–5°N and 120°–160°W. Bold values in the fourth column indicate EPC events according to the 0.70 °C threshold criterion illustrated in Fig. 2d, and normal fonts indicate EPN events. Note that some Niño 3.4 SST values fall below the 0.5 °C criterion that defines El Niño events because the method of calculating anomalies used here differs from that of NOAA CPC, who use 30-year climatologies updated every 5 years

We calculated El Niño-related extratropical composites of various reanalysis and observational datasets of both seasonal and daily resolution, focusing on the domain poleward of 10°N and from 160°E eastward to 40°E. This domain encompasses the Pacific/North American and the North Atlantic/western European regions. To examine the upper tropospheric circulation, we focus on 300 hPa geopotential height (Z300) and streamfunction from the National Centers for Environmental Prediction–National Center for Atmospheric Research (NCEP–NCAR) reanalysis (Kalnay et al. 1996) and from the ERA-Interim reanalysis (Dee et al. 2011). The reason for using two different sources is that the NCEP–NCAR reanalysis extends back to the first year of the analysis, 1950, and so we use monthly mean NCEP–NCAR reanalysis data for the seasonal composites. The ERA-Interim reanalysis data, which only extend back to 1979, are used at daily resolution for the composites that examine the intraseasonal evolution of the El Niño teleconnections in relation to tropical OLR variability. We also use ERA-Interim T2m and precipitation for the intraseasonal composite analysis. We choose the ERA-Interim reanalysis for the intraseasonal analysis because this dataset is of higher spatial resolution (~0.7° vs. 2.5° for NCEP–NCAR reanalysis), is likely to be of higher quality in some regions like the Arctic (Screen and Simmonds 2010), and covers the entire period of the tropical OLR analysis. As shown in the following section, the anomaly patterns are consistent across datasets.

From the NCEP–NCAR reanalysis, we also analyze extratropical 200 hPa zonal wind and anomalies of 2.5—6-day bandpass filtered 500 hPa streamfunction, which is an indicator of storm track variability. We applied two successive applications of a 10-point butterworth filter on the six-hourly 500 hPa streamfunction to retain variance in the 2.5—6-day timescale. The six-hourly data were partitioned into monthly segments for each winter month, and the temporal root mean square (RMS) values were computed for each month. This approach for defining storm track variability is very similar to that of Lau (1988) except that Lau (1988) focuses on 500 hPa geopotential height instead of streamfunction.

For the seasonal composites analysis, we also use the Global Historical Climatology Network (GHCN) and Climate Anomaly Monitoring System (CAMS) land T2m (Fan and van den Dool 2008) and Global Precipitation Climatology Centre (GPCC) V6 precipitation (Schneider et al. 2011, 2013). The GHCN CAMS and GPCC V6 are gridded datasets of 0.5° and 1° spatial resolution, respectively, that are derived from global station data. Although we focus on variables for the winter season of December–March, we also briefly examine monthly mean June–August Palmer Drought Severity Index (PDSI) data (Dai et al. 2004), provided on a 2.5° latitude-longitude grid, to demonstrate that the wintertime contrasts of EPC and EPN El Niño extend to contrasting impacts on summertime droughts and pluvials.

For all El Niño composite calculations except that of 200 hPa zonal wind, we first calculated anomalies by removing the seasonal cycle. For the monthly mean data, the seasonal cycle is defined as the calendar month means for the 1951–2000 period. For the daily data, the seasonal cycle is defined as the first four harmonics of the calendar day means for the 1981–2010 period. We then smoothed the daily anomalies with a 7-day running mean, which helps to emphasize robust features in the composite analysis but does not alter any conclusions. We linearly detrended all anomalies to focus on intraseasonal and interannual variability rather than features that may relate to the long-term trend. The removal of the linear trend also removes any offsets between seasonal cycles defined with different base periods.

2.2 Climate model simulations forced by time-varying SSTs

The limited amount of reliable observational data combined with substantial sampling variability provides a challenge in detecting robust differences in different types of El Niño teleconnections. To supplement our analysis of observational datasets, we analyze several large-ensemble simulations from atmospheric general circulation models (AGCMs) that, in the style of the Atmospheric Model Intercomparison Project (AMIP), are forced by time-varying SSTs. The use of a large ensemble allows us to suppress the noise of internal atmospheric variability when calculating ensemble means for both the EPC and EPN El Niño episodes. We focus on a 40-member ensemble of the Geophysical Fluid Dynamics Laboratory Atmospheric Model version 2.1 (AM2.1; The GFDL Global Atmospheric Model Development Team 2005) that covers the full 1950–2012 period considered in this study. The model uses a finite-volume atmospheric dynamical core with horizontal resolution of ~200 km. Each member of the 40-member ensemble with different initial conditions is forced by ERSST v3b. The sea surface is regarded as 100 % sea-ice covered if SST is equal to or lower than –1.8 °C. Radiative forcing is held constant at 1990 levels. We analyze the 1950–2012 period after a 1-year spin-up of the model.

We also analyze AMIP simulations with observed radiative forcing from five additional models participating in the NOAA Facility for Climate Assessments (FACTS) that cover the 10 El Niño episodes since 1979. These five models, the CAM4, LBNL-CAM5.1 (CAM5.1), ECHAM5, GEOS-5, and ESRL-GFSv2 (GFSv2) have ensemble sizes

Table 2 Description of the FACTS AMIP climate model simulations for the analysis of El Niño episodes between 1979 and 2013

Model name	Source	Horizontal resolution	Vertical resolution	Number of ensemble members	References
CCSM4.0 CAM (CAM4)	National Center for Atmospheric Research (NCAR)	~1.0° × 1.0°	25 layers	20	Neale et al. (2010)
LBNL-CAM5.1 (CAM5.1)	NCAR	~1.0° × 1.0°	25 layers	12	Neale et al. (2012)
ECHAM5	Max Planck Institute for Meteorology (MPI)	0.75° × 0.75°	31 layers	30	Roeckner et al. (2003)
GEOS-5	NASA Goddard Space Flight Center (GSFC)	1.25° × 1.0°	72 layers	12	Molod et al. (2012), Schubert et al. (2014)
ESRL-GFSv2 (GFSv2)	NOAA/NWS Environmental Modeling Center (EMC)	1.0° × 1.0°	64 layers	50	Saha et al. (2014)

Observed, time-evolving radiative forcing is applied to all the simulations

ranging from 12 to 50. A more complete description of these simulations is given in Table 2, and additional information about these experiments is available online at http://www.esrl.noaa.gov/psd/repository/alias/facts.

3 The morphology of EPC and EPN El Niño episodes

In this section we first provide the analysis of tropical SST/deep convection relationships that motivates the EPC/EPN partitioning of this study. Then we present the analysis of seasonal and intraseasonal composites associated with these two El Niño categories.

3.1 The relationship between SSTs and deep convection in the tropical Pacific

As argued in the introduction, if distinct El Niño impacts between unique El Niño episodes, like the 1987/1988 and 1991/1992 events (referred hereafter as the 1988 and 1992 events, as defined by the year of the January–March anomalies) of Fig. 1, are predictable on seasonal timescales, then the predictable variations likely relate to differences in tropical convection. Figure 2a, b illustrate the December–March tropical Pacific OLR anomalies for the 1988 and 1992 events. In addition to the 1992 event being stronger (see Table 1), the patterns of tropical convection are distinct—the 1992 event features enhanced deep convection extending into the eastern equatorial Pacific (an "OLR El Niño" by the Chiodi and Harrison 2013 terminology), whereas the enhanced deep convection is more zonally confined to the western and central equatorial Pacific for the 1988 event. The differences between these two OLR patterns may be understood through a comparison between OLR/SST relationships in the central and eastern equatorial Pacific region. Figure 2c shows a scatter plot of the 1979–2012 DJFM OLR anomalies versus the "relative" SST (RSST), where RSST is defined as the local minus tropical mean (20°S–20°N) SST (the motivation for the use of RSST is explained below) in a central equatorial box (5°S–5°N, 160°E–160°W). The relationship between deep convection and RSST is approximately linear over this region, and the nearly linear relationship between central Pacific OLR and Niño 3 (5°S–5°N, 150°W–90°W) SST is noted in L'Heureux et al. (2015).

Figure 2d illustrates the same relationship in Fig. 2c except for an eastern equatorial Pacific box (5°S–5°N, 160°W–120°W). This particular box is chosen because it captures the maximum in inter-El Niño OLR variance (not shown). In contrast with the central equatorial Pacific, the relationship between deep convection and SST is clearly nonlinear over the eastern equatorial Pacific. Hoerling et al. (1997) describe the nonlinear relationship between deep convection and SST and its role in El Niño/La Niña teleconnection pattern asymmetries, but here we expand upon how the pattern of convection during El Niño depends on both the eastern Pacific SST anomaly and the tropical mean state. Over this eastern Pacific region, the OLR varies little with RSST until a value ~0.7 °C, after which the OLR drops sharply, indicating the onset of deep convection. The linear fit above a threshold in Fig. 2d is obtained through a nonlinear optimization of the threshold and slope parameters, similar to that used in Back and Bretherton (2009) and Johnson and Xie (2010). This sharp increase in convection at an RSST ~0.7 °C, or an absolute SST ~27.9 °C for the 1979–2012 period, corresponds with the well-known SST threshold for convection (Gadgil et al. 1984; Johnson and Xie 2010).

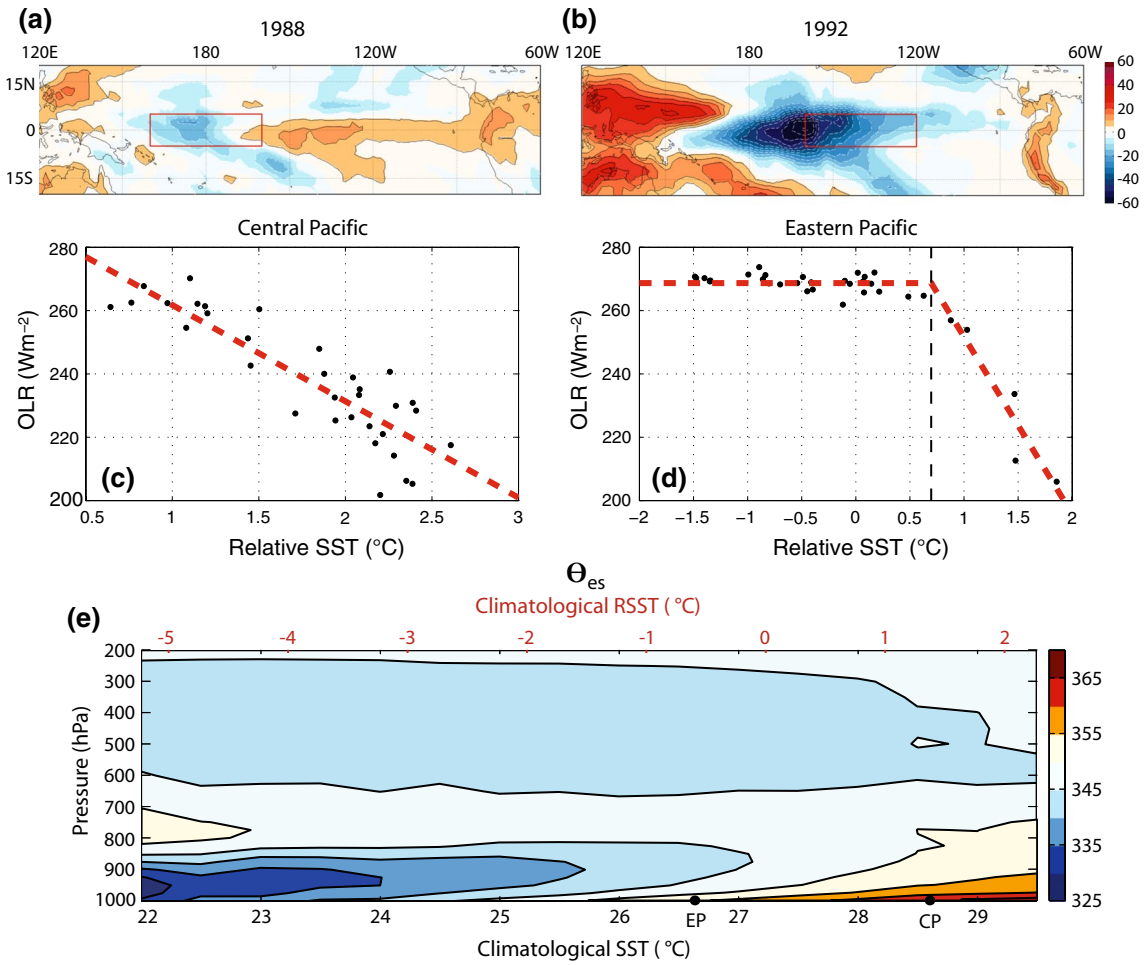

Fig. 2 December–March OLR anomalies (contour interval is 5 W m^{-2}) for the **a** 1988 and **b** 1992 El Niño episodes. **c** Scatter plot of 1979–2012 December–March OLR anomalies averaged over the central Pacific equatorial box (5°S–5°N, 160°E–160°W) shown in **a** as a function of RSST averaged in the same box. The *red dashed line* shows the least squares linear fit. **d** As in **c** but for the eastern equatorial box (5°S–5°N, 160°W–120°W) shown in **b**, and the *red dashed line* is a linear fit above a threshold determined through a nonlinear optimization. The *dashed black line* indicates the RSST threshold. **e** December through March 1979–2013 climatological θ_{es} (contour interval is 5 K) in the deep tropics (20°S–20°N) binned by climatological SST (lower x-axis) at intervals of 0.5 °C and averaged at each pressure level (y-axis). The points labeled "CP" and "EP" correspond with the climatological SST of the *boxes* shown in **a** and **b**, respectively. The upper x-axis indicates the climatological RSST

The physical explanation of this threshold, also discussed in Johnson and Xie (2010), is illustrated in Fig. 2e, which shows how the climatolological θ_{es} over the deep tropics varies with climatological SSTs and RSSTs. As a consequence of the weak free-tropospheric θ_{es} gradients in the deep tropics (e.g., Sobel et al. 2001), conditional instability is closely tied to the boundary layer θ_{es}, which in turn is strongly related to the underlying SSTs. Below a climatological SST of ~27.5 °C, which includes the eastern Pacific box, the atmosphere is conditionally stable above the boundary layer (θ_{es} increases with height above ~850 hPa), inhibiting the initiation of deep convection and rendering the seasonal rainfall insensitive to SSTs until that convective threshold is reached (Fig. 2d). In contrast, the atmosphere of the central Pacific box, with climatological SSTs currently ~28.5 °C, is conditionally unstable throughout a deep layer in the climatology, and so the rainfall varies more linearly with RSST (Fig. 2c).

The relationship between tropical SSTs and conditional instability depends on the mean state, i.e., the free tropospheric temperature in particular, and so both convective threshold and the absolute SST/OLR relationships are expected to be non-stationary. Fortunately, tropical free tropospheric temperatures and the convective threshold vary in close concert with the tropical mean SSTs (Sobel et al. 2002; Johnson and Xie 2010), and so the transformation of absolute SST to RSST yields a more stable relationship with deep convection. This reasoning motivates the use of RSST in Fig. 2. We note that the distinction between RSST and absolute SST is not critical over short

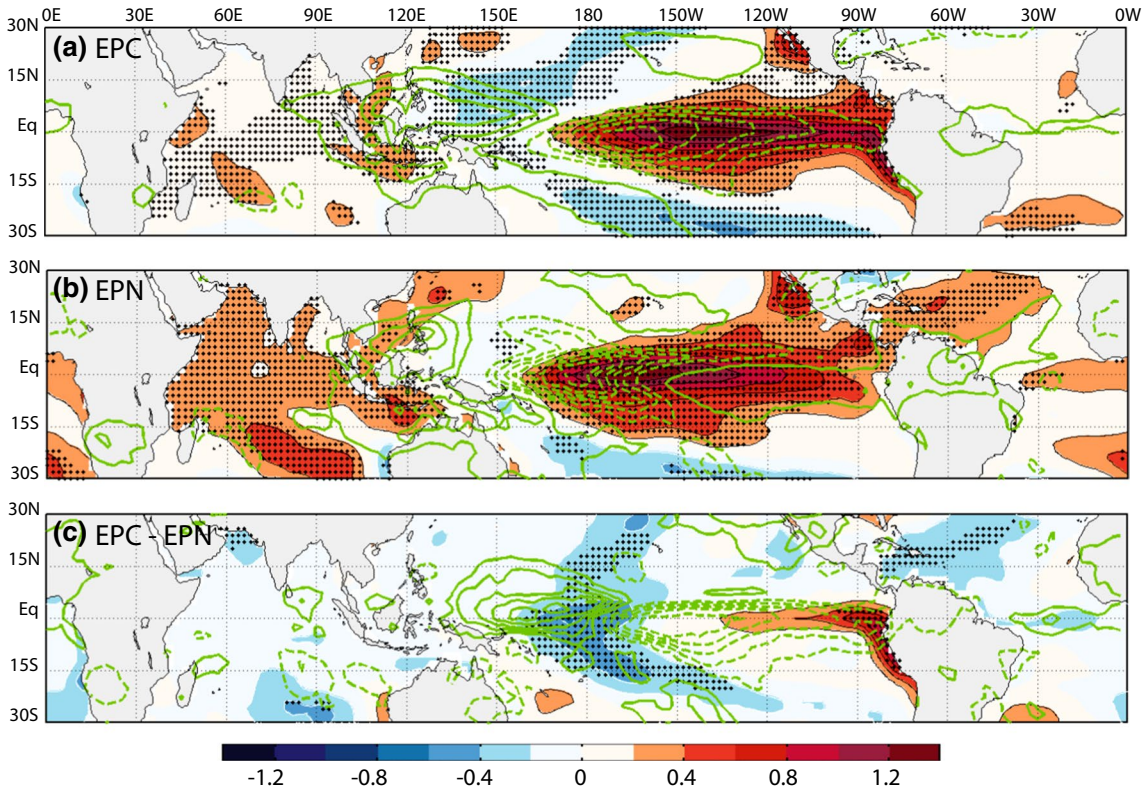

Fig. 3 December–March normalized composite anomalies of SST (*color shading* °C °C^{-1}) and OLR (*green contours* W m^{-2} °C^{-1}), where the normalization is by the mean Niño 3.4 SST anomaly amplitude, for **a** EPC and **b** EPN El Niño episodes. The mean Niño 3.4 SST anomalies are 1.59 and 0.63 °C for EPC and EPN episodes, respectively. **c** The difference between the EPC and EPN El Niño composites (**a** minus **b**). The SST composites cover all El Niño episodes between 1950 and 2013, whereas the OLR composites cover the period between 1979 and 2013. OLR anomalies are contoured at intervals of 5 W m^{-2}, with *dashed* (*solid*) contours indicating negative (positive) OLR anomalies and the zero contour is omitted. *Stippling* indicates SST anomalies are statistically significant at the 5 % level on the basis of a two-sided *t* test

time periods of a few decades when tropical eastern Pacific SST variance is large relative to that of tropical mean SST, but this distinction becomes important over longer periods when the long-term change in tropical mean SSTs may be comparable to that of local, seasonal SST deviations (see, for example, Xie et al. 2010). Most importantly for the present purposes, a clear physical understanding of the relationship between local SST, tropical mean SST, and OLR gives us confidence to extend our analysis to time periods before 1979 when OLR or satellite-derived rainfall is unavailable.

3.2 Partitioning into EPC and EPN events

The preceding analysis and the discussion in the introduction lead us to hypothesize that El Niño episodes with eastern Pacific RSSTs that cross the convective threshold (EPC episodes) yield wintertime teleconnection patterns that are distinct from those episodes that do not (EPN episodes). To explore this hypothesis, we partition the 21 El Niño episodes from 1950 to 2013 into EPC and EPN categories according to the eastern Pacific RSST criterion illustrated in Fig. 2d: those El Niño events with a December–March eastern Pacific RSST exceeding 0.7 °C fall in the EPC category, and all others are EPN events. This criterion yields 8 EPC and 13 EPN events listed in Table 1.

We first examine the difference in the SST and OLR anomaly patterns between EPC and EPN events through an analysis of normalized composites (Fig. 3). Each composite has been normalized by the mean Niño 3.4 SST anomaly amplitude for the category to enable focus on the difference in the spatial patterns rather than the larger amplitude of the EPC events (analogous to a one-sided linear regression). By first focusing on the SST anomaly patterns, we see that the EPN SST anomalies tend to be centered about 30° west of the EPC SST anomalies, which suggests a tendency for EPN events to coincide with the Central Pacific flavor of El Niño. This difference also is consistent with stronger events generally centered farther east (Takahashi et al. 2011; Capotondi et al. 2015). Table 1 indicates both the EPC/EPN and EP/CP categories of each El Niño episode, where the EP/CP distinction is based on the consensus categorization

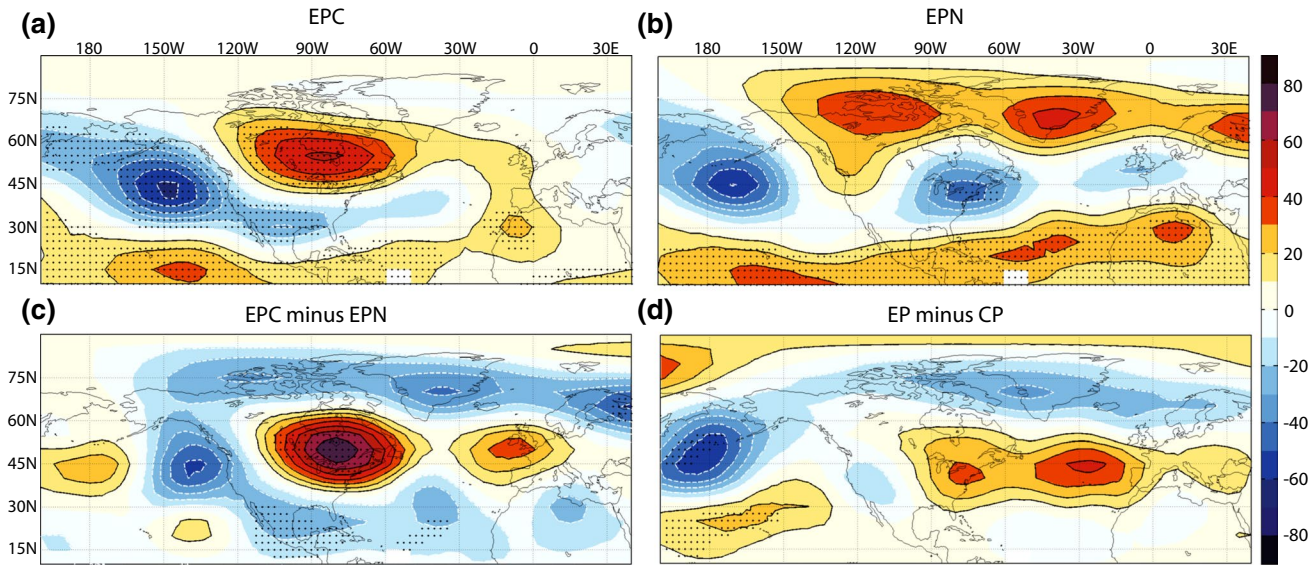

Fig. 4 December–March composite anomalies of 300 hPa geopotential height anomalies (m $°C^{-1}$), normalized by the mean Niño 3.4 SST anomaly amplitude, for **a** EPC and **b** EPN El Niño episodes. *Stippling* indicates anomalies that are statistically significant at the 5 % level on the basis of a two-sided *t* test. *Bottom panels* indicate the difference in normalized 300 hPa geopotential height anomalies **c** between EPC and EPN composites and **d** between EP and CP composites. *Stippling* indicates normalized differences that are statistically significant at the 5 % level on the basis of a two-sample *t* test

of Yu et al. (2012). Overall, there is a moderate degree of overlap, with four of eight EPC events in the EP category, and nine of 13 EPN events in the CP category. However, there also are clear distinctions in the two types of partitioning, and as discussed in the introduction, there is considerable variation in the partitioning between EP and CP categories depending on the particular methodology. Moreover, Fig. 3 indicates that the composite SST differences between EPC and EPN events are not as dramatic as the differences in OLR, with composite negative OLR anomalies extending all the way to the South American coast for EPC events but confined to the central and western equatorial Pacific for EPN events. These patterns are consistent with the arguments presented in the previous section.

To investigate the differences between EPC and EPN teleconnection patterns, we next examine the differences in upper tropospheric structure through composites of Z300 anomalies, normalized by the Niño 3.4 SST anomaly amplitude in the same way as in the SST composites (Fig. 4). Consistent with the hypothesis presented above, we see notable differences in the upper tropospheric structure between EPC and EPN events. The composite for EPC events features a deepened and eastward displaced Aleutian low, positive height anomalies over the subtropical Pacific, positive height anomalies extending across northern North America, and negative height anomalies extending across southern North America (Fig. 4a). This pattern resembles the classic El Niño teleconnection pattern (e.g., Trenberth et al. 1998) that projects onto the positive phase of the Pacific/North American (PNA) pattern as well as the negative phase of the Tropical/Northern Hemisphere (TNH) pattern (Mo and Livezey 1986; Livezey and Mo 1987; Peng and Kumar 2005). Statistically significant anomalies in the extratropics generally are confined to the Pacific/North American region.

The EPN Z300 anomaly pattern, in contrast, features a deepened Aleutian low that is displaced farther to the west, an anomalous ridge over western North America, and significant negative anomalies over northeastern North America (Fig. 4b). Over the North Atlantic and European region, the pattern appears to project onto the negative phase of the NAO and Arctic Oscillation (AO), although the composite anomalies are only significant over a small area of northern Europe. The EPN Z300 composite pattern over Europe agrees with the El Niño composite high-over-low dipole pattern reported in previous studies (e.g., Fraedrich and Müller 1992), possibly suggesting that the canonical response over Europe may be more closely associated with EPN events. The difference between the EPC and EPN Z300 composites (Fig. 4c) illustrate largest differences over northeastern North America, and statistically significant differences cover a large fraction of North America. Because several episodes—1969, 1977, 1995, 2003, and 2010—may be considered borderline with respect to the RSST criterion used in this partitioning (see Table 1), we repeated the composite calculations after excluding these cases. The results (not shown) are similar to what we show in Fig. 4 but with the area of statistically significant

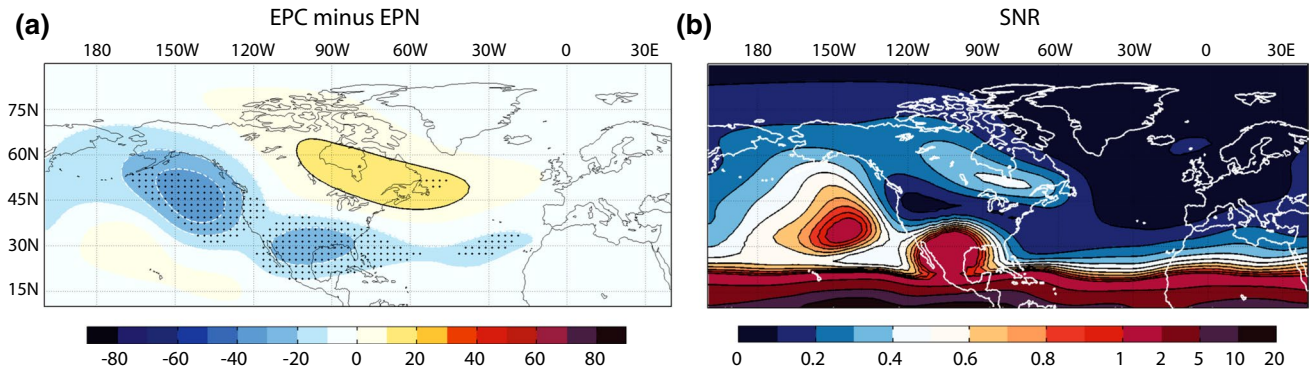

Fig. 5 **a** As in Fig. 4c but for the ensemble means of the 40-member AMIP-type AM2.1 simulations. **b** Ratio of variance of the Z300 AM2.1 ensemble means to the variance of the individual ensemble members about the ensemble means for the 21 El Niño episodes listed in Table 1

differences increasing, which indicates that these conclusions are even more robust if we omit borderline EPC and EPN episodes.

To compare these features with the more commonly studied EP/CP El Niño distinctions, we performed the same Z300 composite difference calculations but for EP and CP El Niño events, which are illustrated in Fig. 4d. Most notably, and in contrast with the EPC/EPN partitioning, the normalized composite Z300 differences between EP and CP events are not statistically significant over North America, northern Africa, or Europe. In agreement with Chiodi and Harrison (2013, 2015), this result suggests that the partitioning between EPC and EPN events is more fundamental than the partitioning between EP and CP events from the perspective of Northern Hemisphere, wintertime teleconnection patterns. In contrast with Chiodi and Harrison (2013, 2015), we argue that this partitioning may occur through an RSST threshold condition that allows us to extend the analysis before the satellite era. This finding does not suggest that the partitioning between EP and CP El Niño events is not meaningful or that the teleconnection patterns of EP and CP El Niño events are identical; it is likely that significant differences would emerge as sample sizes increase (Yu et al. 2012). Moreover, as mentioned above, the distinction between EP and CP "flavors" of El Niño is a contributing factor to the distinction between EPC and EPN events. This result, however, does highlight that the dynamics and predictability of El Niño teleconnection patterns may be more closely tied to the nonlinear relationship between SST and deep convection in the eastern equatorial Pacific Ocean than to the distinction between EP and CP events.

Because the numbers of EPC and EPN events in the observational record are limited, some of the features evident in Fig. 4 may not be robust. In order to investigate the robustness of the Z300 teleconnection pattern differences, we performed the same Z300 difference calculations but with the ensemble means of the 40-member AMIP-type AM2.1 simulations (Fig. 5a). These simulations exhibit very similar eastern Pacific precipitation threshold behavior as in observations (not shown). By taking the mean of 40 ensemble members, we average out most of the noise of internal atmospheric variability in the model and isolate the SST-forced atmospheric response. A comparison of Fig. 4c with Fig. 5a reveals notable similarities, including negative Z300 differences over the northeastern Pacific and southern North America and positive differences over northeastern North America. This Z300 difference pattern likely is related to the third empirical orthogonal function (EOF) of SST-forced geopotential height variability identified by Kumar et al. (2005) in a similar AMIP-type large-ensemble AGCM experiment. The positive differences over northeastern North America, however, are not as large as in observations; the mismatch in amplitude over northeastern North America may be the result of model error, sampling variability in observations, or a combination of the two. Nevertheless, the overall similarity in the patterns increases confidence that observed differences in EPC and EPN teleconnection patterns are robust.

For the AM2.1 simulations we also assess the potential predictability of El Niño teleconnection pattern variations by comparing the SST-forced Z300 variance (the external variance) with the internal variance for all 21 El Niño episodes. Following Kumar and Hoerling (1995) but for the subset of El Niño episodes, we define the external variance as

$$\sigma_E^2 = \frac{1}{M}\sum_{\alpha=1}^{M}\left(\bar{A}_\alpha - \bar{A}\right)^2, \tag{2}$$

where $\bar{A}_\alpha$ is the ensemble mean Z300 for El Niño episode α, $\bar{A}$ is the grand mean for all 21 El Niño episodes, and M is the total number of El Niño episodes (21). The external variance estimates the amount of Z300 variance that may

be attributed to different El Niño flavors. Following Kumar and Hoerling (1995) again, we define the internal variance as

$$\sigma_I^2 = \frac{1}{MN}\sum_{\alpha=1}^{M}\sum_{i=1}^{N}\left(A_{i\alpha} - \bar{A}_{\alpha}\right)^2, \quad (3)$$

where $A_{i\alpha}$ indicates ensemble member i for El Niño episode α, and N is the total number of ensemble members (40). The internal variance estimates the variance attributed to random weather variations unassociated with the underlying SSTs. The ratio of external to internal variance provides a "signal-to-noise" ratio (SNR) that describes the ratio of Z300 variance that is potentially predictable by the SST variations within El Niño episodes (Fig. 5b). This ratio is <0.5 over most of the domain, which supports previous studies suggesting that most of the inter-El Niño variability in observations is attributable to atmospheric internal variability (Hoerling and Kumar 1997; Kumar and Hoerling 1997). Nevertheless, there are regions, most notably over the northeastern Pacific and southern North America, where the SNR indicates a substantial amount of potentially predictable, SST-forced variability. Moreover, this SNR pattern resembles the EPC minus EPN composite (Fig. 5a) in the extratropics, suggesting that the EPC/EPN partitioning is capturing much of the inter-El Niño SST-forced variability in the model. The largest differences between Fig. 5a, b are found in the tropics, where the SNR is large but the normalized EPC minus EPN composite amplitudes are weak. This difference reflects the influence of El Niño amplitude differences, which lead to high SNR in the tropics that are not captured in the composite in Fig. 5a because of the normalization by Niño 3.4 SST amplitude. Overall, the AM2.1 simulations support that EPC/EPN teleconnection pattern differences are robust, and that this distinction may account for much of the potentially predictable variations in wintertime El Niño teleconnection patterns.

To evaluate the robustness of this relationship in other models but for a more limited time period (1979–2013), we show the EPC minus EPN normalized Z300 differences for five other climate models from the FACTS database (Fig. 6). We also reproduce the analysis derived from reanalysis and AM2.1 data for the shorter period (Fig. 6a, g), which agrees well with the pattern that emerges over the longer period (Figs. 4c, 5a). Figure 6 reveals that all six models capture the overall pattern of EPC/EPN El Niño differences that are evident in reanalysis data (Fig. 6g). The primary sources of disagreement among the models relate to the strength of the differences in several action centers, particularly over the central North Pacific, northeastern North America, and the Arctic. The short observational record does not allow us to determine which models capture this nonlinearity in the teleconnection pattern most accurately, but it is reassuring that all models at least capture the general pattern, increasing confidence that our state-of-the art climate models can capture these distinct "flavors" of the El Niño teleconnection.

In order to provide more context with regard to how the individual El Niño episodes comport with the composite calculations, we calculated the centered pattern correlation between each of the 21 1950–2013 El Niño December–March PNA region (10°–90°N, 180°–30°W) Z300 anomaly fields and both the EPC and EPN Z300 composite fields. We performed these calculations for both the reanalysis data and AM2.1 ensemble mean. The results, presented as a function of eastern Pacific RSST (Fig. 7), demonstrate a general consistency with the arguments presented above: all eight of the EPC events have a higher pattern correlation with the EPC composite than with the EPN composite, and 10 out of 13 (nine out of 13) of the EPN events have a higher pattern correlation with the EPN composite than with the EPC composite in the reanalysis data (AM2.1 simulations). Moreover, the transition of higher pattern correlation from the EPN to EPC composite occurs at an eastern Pacific RSST of ~0.7 °C, although the reanalysis data indicate that the transition may occur at a slightly lower RSST. However, the variability in pattern correlation is large, especially for the EPN episodes that have a weaker SST-forced signal, and so the data are insufficient to distinguish a more refined estimate of this transitional RSST. As expected, the AM2.1 ensemble means generally feature higher pattern correlations, and the EPC/EPN composite pattern correlation differences are not as large as in reanalysis data, which reflects the weaker composite differences in the AM2.1 (Figs. 4, 5 and the higher horizontal red line for AM2.1 in Fig. 7). Interestingly, a couple of El Niño episodes (1952 and 1959) have low pattern correlations (<0.4) in both the reanalysis and AM2.1, which suggests that the SST-forced atmospheric circulation response for those episodes, at least in the AM2.1, either reflects different flavors of ENSO not captured here or SST forcing unrelated to ENSO. Nevertheless, Fig. 7 suggests that the differences evident in the Z300 composite differences hold for many of the individual El Niño episodes.

We also calculated the EPC/EPN normalized composites and their differences for observed T2m and precipitation (Fig. 8). For the EPC composites, positive T2m anomalies extend across most of Canada and the northern tier of the U.S. (Fig. 8a). For EPN composites, in contrast, the positive T2m anomalies are more confined to western North America, whereas negative anomalies dominate eastern North America, although only isolated composite T2m anomalies are statistically significant (Fig. 8c). This lack of statistical significance in the EPN seasonal mean composites is consistent with Chiodi and Harrison (2013, 2015). However, as we discuss in the next section, this pattern

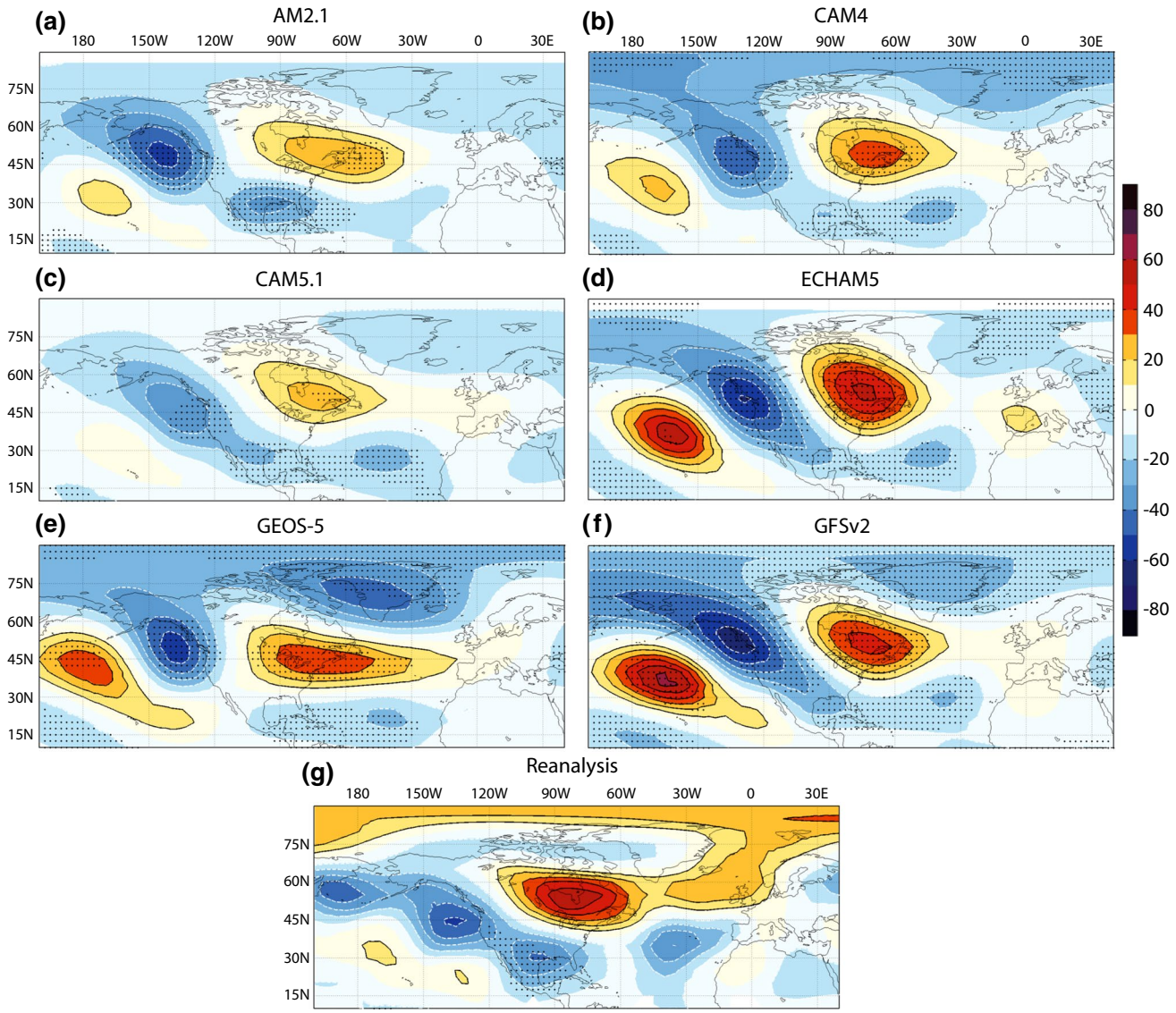

Fig. 6 As in Fig. 4c but for the ensemble means of the AMIP-type simulations of the **a** AM2.1, **b** CAM4, **c** CAM5.1, **d** ECHAM5, **e** GEOS-5, and **f** GFSv2 and for the **g** reanalysis data. The analysis covers the 10 El Niño episodes from 1979 to 2013

of T2m anomalies is more robust when we consider variations on intraseasonal timescales. Another notable difference is found over Arctic regions, where EPC events tend to be associated with negative anomalies but EPN events are associated with positive anomalies, even over northern Europe. This observation is discussed further in Sect. 4.2.

The precipitation composites show even more striking differences. EPC El Niño episodes are associated with much wetter conditions over the southern U.S., with dry anomalies to the north (Fig. 8b). EPN episodes are much drier overall, especially in the southeastern U.S. but apparently over parts of northeastern Europe as well (Fig. 8d). We note that the general patterns of EPC/EPN differences are similar to the differences noted between EP and CP El Niño flavors, for both temperature (Yu et al. 2012) and precipitation (Yu and Zou 2013), but, as with Z300, the composite differences are stronger between EPC and EPN events (not shown). This again argues for a more fundamental partitioning between EPC and EPN categories. Finally, we note that the anomalies for the 1988 and 1992 events shown in Figs. 1 and 2 bear a strong resemblance to the composites for EPN and EPC categories, respectively, supporting that some of the climate anomaly differences between the two events are attributable to the different SST and tropical convection patterns and, therefore, are potentially predictable.

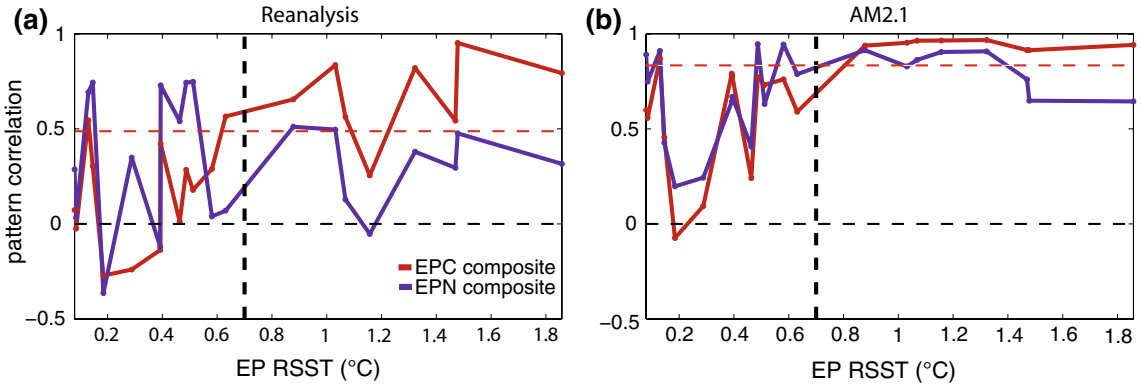

Fig. 7 Centered pattern correlations (y-axis) between each of the 21 1950–2013 El Niño DJFM PNA region (10°–90°N, 180°–30°W) Z300 anomaly fields and the EPC (*red*) and EPN (*blue*) Z300 composite fields for **a** reanalysis data and **b** the AM2.1 ensemble mean as a function of eastern Pacific RSST (x-axis). The eastern Pacific RSST is averaged over the *box* shown in Fig. 2, and the *vertical line* at RSST = 0.7 °C is the threshold determined by the analysis in Fig. 2. The *horizontal red lines* are the pattern correlations between the EPC and EPN Z300 composites (0.49 in the reanalysis and 0.83 in the AM2.1)

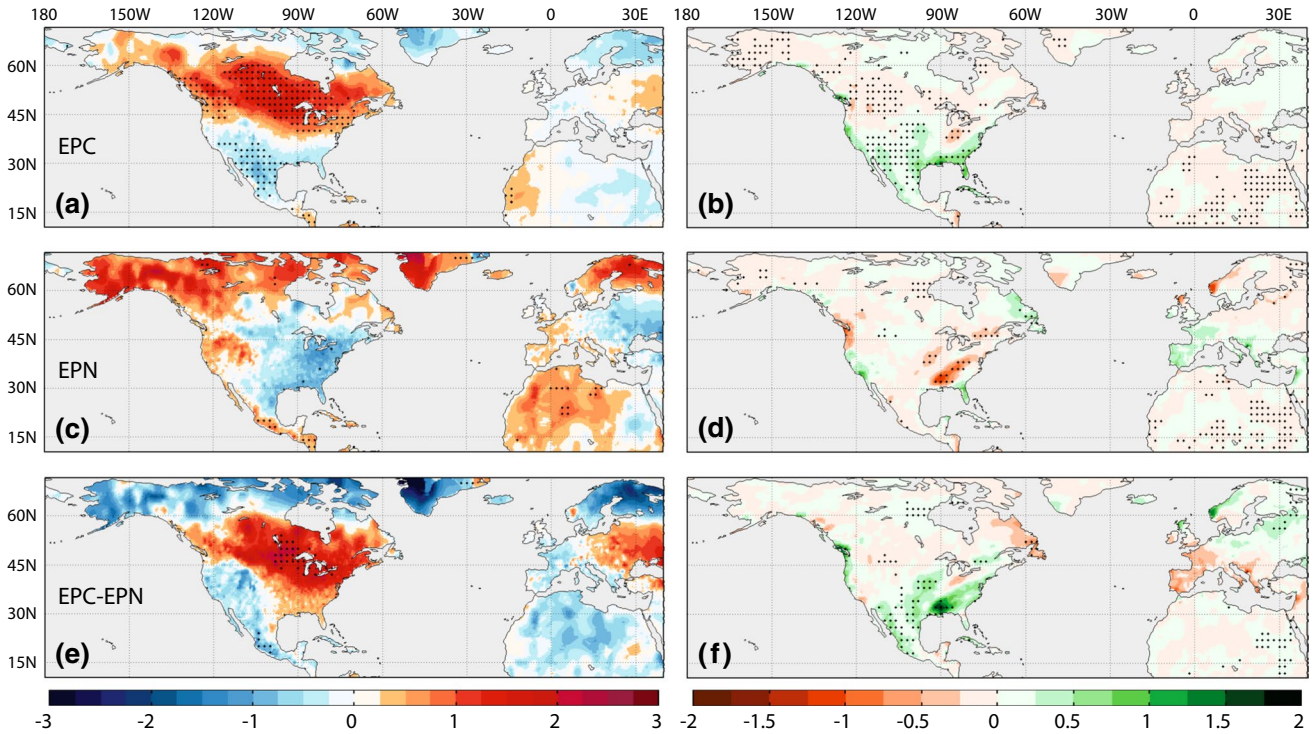

Fig. 8 December–March composite anomalies of **a**, **c** T2m (°C °C^{-1}) and **b**, **d** precipitation (mm d^{-1} °C^{-1}) anomalies, normalized by the mean Niño 3.4 SST anomaly for **a**, **b** EPC and **c**, **d** EPN El Niño episodes. *Bottom panels* show the EPC minus EPN normalized composite differences for **e** T2m and **f** precipitation. *Stippling* indicates **a**–**d** composite anomalies or **e**, **f** differences that are statistically significant at the 5 % level based on a two-sided Student's *t* test

3.3 Intraseasonal variability

Although the composite maps shown in the previous section indicate El Niño-related predictability on seasonal timescales, many of the dynamical processes associated with the PNA region teleconnection patterns occur on much shorter intraseasonal timescales (Feldstein 2000, 2002; Johnson and Feldstein 2010). This property motivates us to examine the intraseasonal variability of the tropical convection, Z300, T2m, and precipitation patterns associated with EPC and EPN events. This analysis has the potential advantage of isolating times on the order of a few weeks

when the SNR is higher than on seasonal timescales, which provides an opportunity to improve our understanding of the robustness, dynamical mechanisms, and intraseasonal predictability associated with the EPC and EPN teleconnection patterns.

To examine the intraseasonal evolution of the EPC and EPN teleconnection patterns, we isolate times when intraseasonal tropical OLR anomalies project strongly onto the seasonal mean OLR anomaly patterns. Specifically, we define an EPC and EPN projection time series as the standardized projection of the 7-day running mean tropical OLR anomalies onto the seasonal mean EPC and EPN OLR anomaly patterns, respectively, that are shown in Fig. 3. The standardization is calculated with the mean and standard deviation for all winters from 1979 to 2012, but the analysis only focuses on El Niño episodes. Then we define intraseasonal EPC and EPN events when the projection time series exceeds 1.5 standard deviations. For a sequence of consecutive days exceeding this threshold, the day with the peak threshold is designated as lag 0. To preserve some degree of independence between intraseasonal events, we add the condition that all identified event peaks must be separated by at least 20 days; if this criterion is not met, then we only keep the event with the higher peak amplitude. We emphasize that, unlike the analysis of seasonal mean anomalies, the analysis of intraseasonal variability is confined to the EPC and EPN events since 1979.

We first examine the intraseasonal variability of the OLR anomaly patterns within EPC and EPN episodes (Fig. 9). The lagged composite amplitude time series in the top panels exhibit substantial intraseasonal growth and decay, especially for EPN episodes (Fig. 9b). The EPC events, however, show greater persistence of the OLR anomaly pattern, which may relate to the stronger SST anomaly amplitudes and the eastward extension of convection anomalies into regions that are normally convectively inactive. The convection pattern features an east–west dipole that intensifies from lag −15 days (Fig. 9c) to lag 0 (Fig. 9g), with anomalous convection expanding eastward toward the South American coast. For the EPN events, the growth and decay are more dramatic, and the convection anomalies are confined to the central and western Pacific. In addition, the growth features an intensification of the South Pacific Convergence Zone (Fig. 9f, h). Overall, the peak OLR anomalies during EPN events are only ~30 % weaker than those of EPC events but they are considerably less persistent, undergoing substantial growth and decay over the course of ~30 days.

The intraseasonal evolution of the OLR anomalies may relate to constructive and destructive interference with intraseasonal modes of variability like the Madden–Julian Oscillation (MJO; Madden and Julian 1971). To examine the possible role of the MJO, we calculated lagged composites of the Wheeler and Hendon (2004) MJO index corresponding with the OLR projection time series. The Wheeler and Hendon (2004) MJO index is based on the first two principal components of a combined EOF of tropical OLR and upper- and lower-tropospheric zonal winds. The phase space spanned by these two principal components, designated as RMM1 and RMM2, define eight MJO phases (see Fig. 10a), with MJO episodes typically exhibiting a counterclockwise rotation within this phase space over the course of 30–70 days. We illustrate the composites of daily RMM1 and RMM2 values from lag −20 to lag +20 days for EPC and EPN OLR events in Fig. 10a. We see that the intraseasonal progression of OLR anomalies for both EPC and EPN episodes indeed are associated with statistically significant MJO signatures progressing in a counterclockwise manner. For EPC episodes, the MJO progresses from phase 7 through phase 3 from lag −10 to lag +20 days, with lag 0 corresponding with phase 1. For EPN episodes, the MJO composite amplitudes generally are less significant, but we see a significant progression from phases 5 through 7 from lag −10 days to lag 0. We return to the possible role of the MJO on the composite Z300 anomalies below.

Figures 11 and 12 illustrate the corresponding evolution of 7-day running mean Z300 anomalies for EPC and EPN events, respectively, from lags of −10 to +20 days with respect to the peak OLR pattern amplitudes. Consistent with the persistent OLR anomalies, the composite pattern of Z300 anomalies for EPC events is fairly persistent throughout the 30-day interval (Fig. 11). However, between a lag of −10 to +10 days, we see an intensification and eastward shift of the Aleutian low anomaly as well as a strengthening and westward extension of the North American high anomaly. The peak response occurs at a lag of ~+10 days, and the resulting pattern (Fig. 11d) strongly resembles the seasonal mean Z300 composite for EPC events (Fig. 4a) but with significant negative Z300 anomalies over Greenland and the North Atlantic. The 10-day lag between the OLR anomalies and the peak extratropical response agrees well with previous studies (e.g., Hoskins and Karoly 1981; Jin and Hoskins 1995). The Z300 anomalies over Europe are variable and not statistically significant at most lags.

The evolution of the EPN Z300 anomalies (Fig. 12a, b) is not that distinct from that of EPC events over the PNA region for lags between −10 and 0 days. However, we begin to see notable differences from lag 0 to lag +20 days. The peak response develops between a lag of +5 to +10 days, which features many of the elements evident in the EPN seasonal mean composite (Fig. 4b): a strengthened Aleutian low and North American high that are more westerly displaced than in EPC events, negative Z300 anomalies over eastern North America, and a tripole

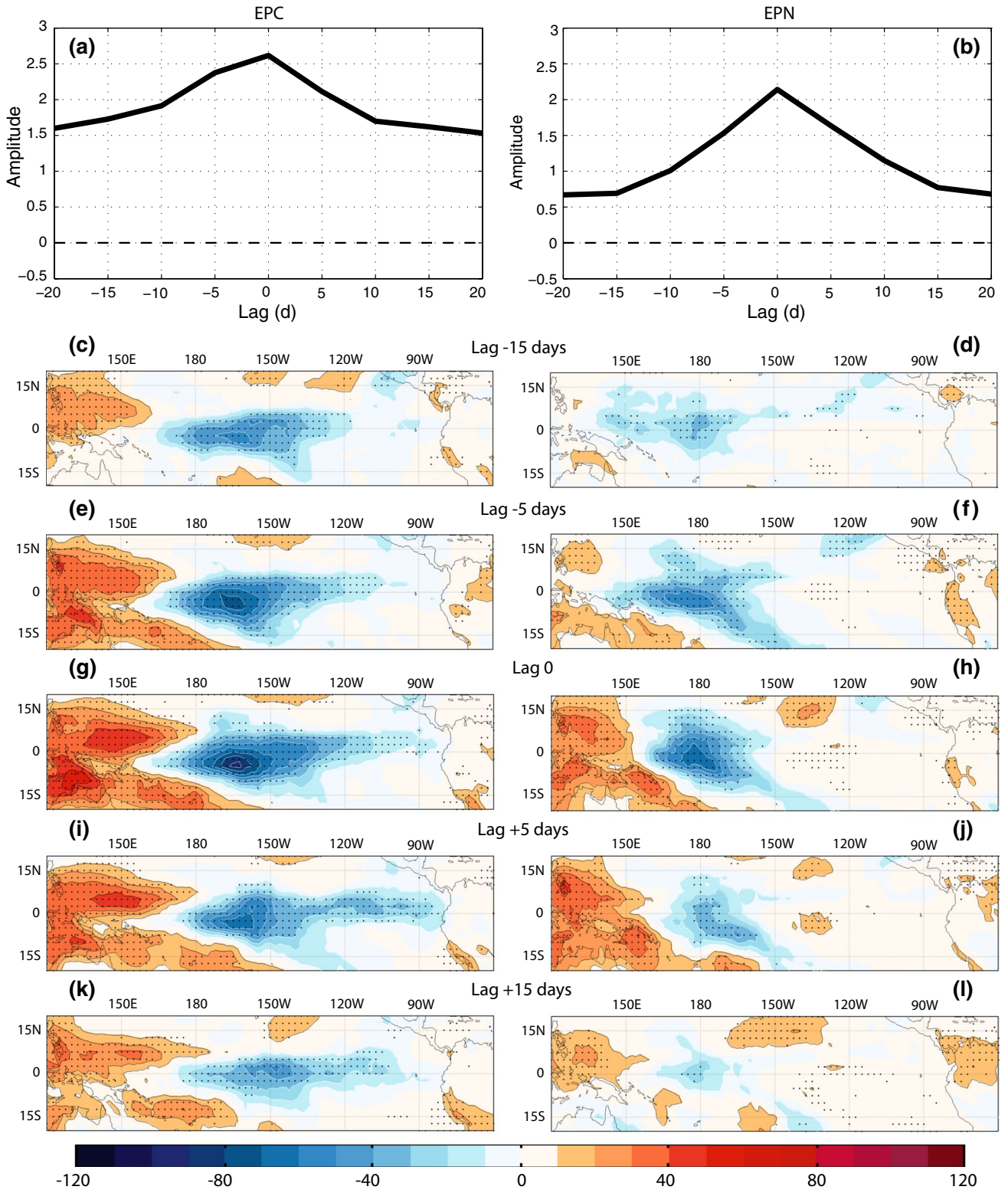

Fig. 9 Lagged composite amplitudes of the 7-day running mean OLR projection time series for December–March **a** EPC and **b** EPN El Niño episodes since 1979. A lag of 0 days represents the middle of the week that defines the peak of the event. The panels below show the **c**, **e**, **g**, **i**, **k** EPC and **d**, **f**, **h**, **j**, **l** EPN composite OLR anomaly patterns (W m^{-2}) for **c**, **d** lag −15, **e**, **f** lag −5, **g**, **h** lag 0, **i**, **j** lag +5, and **k**, **l** lag +15 days. *Stippling* indicates statistically significant OLR anomalies at the 5 % level

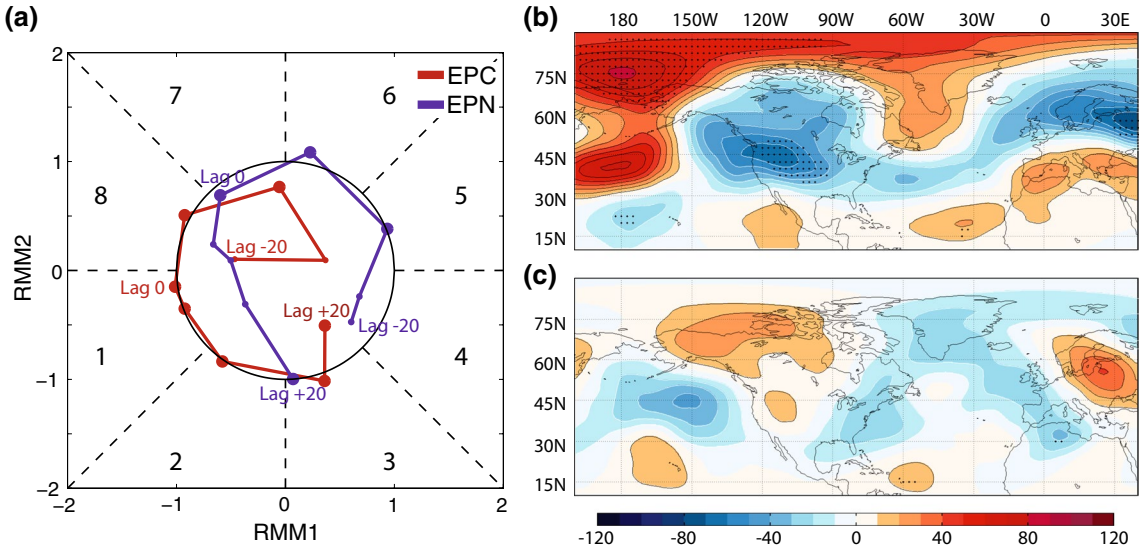

Fig. 10 **a** Lagged composites of daily RMM1 and RMM2 amplitude corresponding with intraseasonal OLR events for EPN (*blue*) and EPC (*red*) El Niño episodes for lags between −20 and +20 days. Points are plotted at 5-day intervals and large points indicate that the distance from the origin is statistically significant at the 5 % level. The inner circle corresponds with an MJO amplitude of 1, and the eight Wheeler and Hendon (2004) MJO phases are labeled. **b** Composite 7-day Z300 anomalies 10 days after MJO index values are close to the lag 0 composite values for EPC OLR events. Here, "close" is define as a distance of <0.2 from the values plotted in **a**. **c** As in **b** but for EPN OLR events. *Stippling* in **b** and **c** indicates statistical significance at the 5 % level

Z300 pattern over the North Atlantic, western Europe, and northern Africa. At lag +5 days, the composite consists of two similar arching wave trains, one over the PNA sector and another over the North Atlantic and Western Europe. However, unlike in the seasonal mean composites, the composite anomalies at these intraseasonal timescales are statistically significant over a large fraction of the domain. This result suggests that many of the features evident in the seasonal mean composite (Fig. 4b) are robust but generally transient throughout the season. Between lag +15 and +20 days, the most salient feature is a band of positive Z300 anomalies extending throughout much of the Arctic, whereas the midlatitude anomalies gradually decay.

We may wonder if the Z300 evolution in Figs. 11 and 12 is simply a reflection of the MJO progression evident in Fig. 10a. To explore this possibility, we identify all winter days when the MJO index is "close" to the lag 0 composite values shown in Fig. 10a. Here, we define "close" as having a distance of <0.2 from the composite values in the MJO phase space (results are not sensitive to the precise threshold chosen). We also impose a 20-day separation criterion and only keep the day with the smallest distance for any sequences that do not meet this criterion. Because the peak response to the OLR anomalies appears to occur with a lag of about 10 days, we calculate the 7-day mean Z300 composite anomalies centered at lag +10 days, as in Figs. 11d and 12d but for the days that meet the MJO distance criteria described above. These composite plots, shown in Fig. 10b, c, indicate that the EPC and EPN Z300 composites are not a strong reflection of the MJO response. For EPC episodes, the Z300 relationship with the OLR projection time series (Fig. 11d) is actually *opposite* to the expected MJO response (Fig. 10b) over large parts of the domain, especially over north-central North America. This result raises an interesting possibility that MJO teleconnection patterns may be distinct during the stronger, EPC El Niño episodes. However, investigation of this hypothesis is beyond the scope of this study. For EPN episodes, the Z300 composites do suggest constructive interference between the MJO and El Niño signal (note the similarity between Figs. 10c and Fig. 12d). The amplitudes of the Z300 composite anomalies in Fig. 10b, however, are much smaller than the amplitudes in Fig. 12d, which again suggests that the MJO is not sufficient to explain the relationships evident in Fig. 12.

The increased robustness of the subseasonal composites relative to the seasonal composites, especially for EPN events, likely relates to the increased SNR on intraseasonal timescales. As an illustration of this point, we calculated the ratio of composite OLR anomaly amplitudes to the standard deviation of OLR anomalies for both EPC and EPN El Niño episodes. For the seasonal mean analysis, we used the seasonal mean OLR composite anomalies (Fig. 3) and the seasonal mean standard deviations for all available winters. For the subseasonal analysis, we used the lag 0 composite OLR anomalies (Fig. 9) and the standard deviation of 7-day OLR anomalies for all available winters. These calculations, shown in Fig. 13, demonstrate that

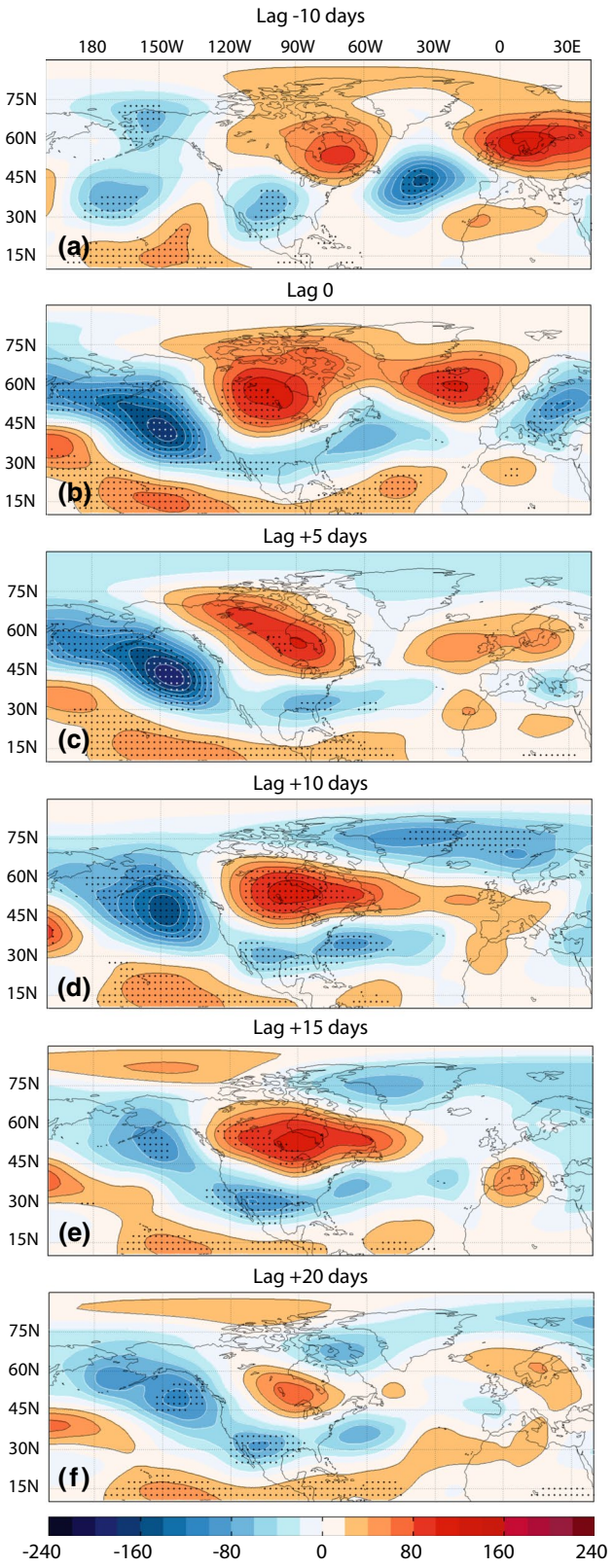

Fig. 11 Lagged composites of the 7-day averaged 300 hPa height anomalies (m) for intraseasonal EPC OLR events at a lag of **a** −10, **b** 0, **c** +5, **d** +10, **e** +15, and **f** +20 days. *Stippling* indicates anomalies that are statistically significant at the 5 % level

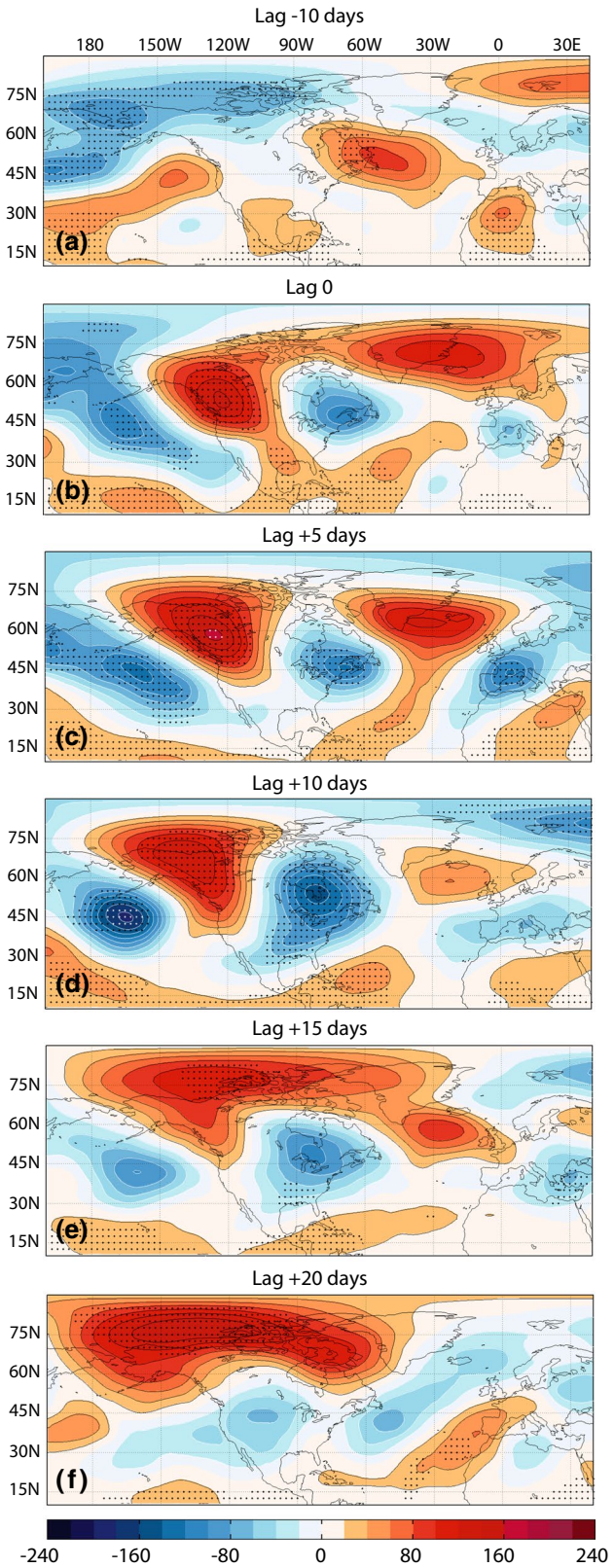

Fig. 12 As in Fig. 11 but for intraseasonal EPN OLR events

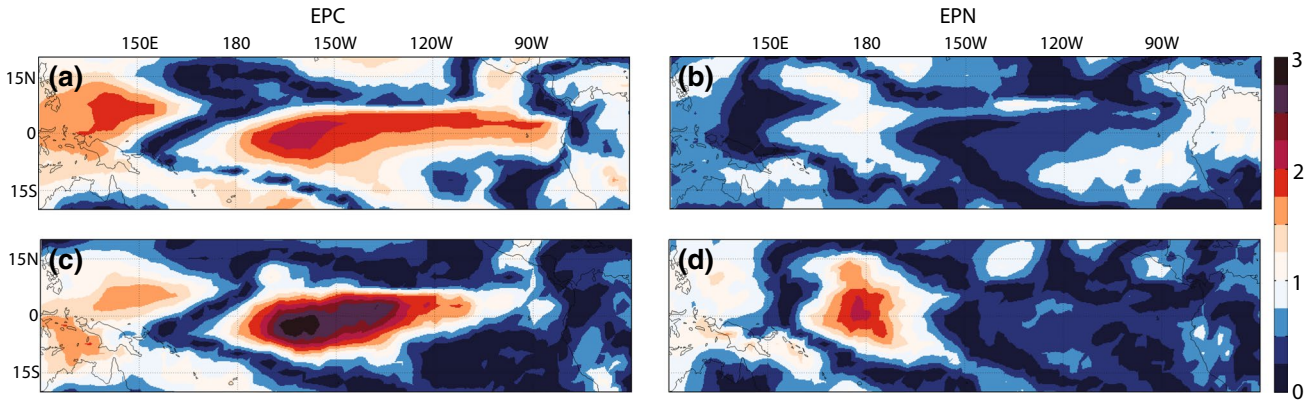

Fig. 13 Ratio of seasonal mean composite OLR anomaly amplitudes to seasonal mean OLR standard deviations for **a** EPC and **b** EPN El Niño episodes. **c**, **d** As in **a** and **b** but for the lag 0 7-day composite OLR anomaly amplitudes of intraseasonal **c** EPC and **d** EPN OLR events divided by the 7-day OLR standard deviations

the peak ratios increase by ~50 % for EPC episodes and ~100 % for EPN episodes on subseasonal relative to seasonal timescales.

Most of the features in the corresponding composite T2m anomaly evolution (Figs. 14, 15) mirror the composite Z300 anomaly evolution. In particular, we see peak T2m anomaly patterns at a lag of 10 days (Figs. 14d, 15d). Once again, the magnitude and fractional area of statistically significant composite anomalies in association with EPN events are much greater on these shorter timescales than on seasonal timescales. For example, the 7-day mean T2m anomalies over eastern North America centered at lag +10 days range from about −2 to −4 °C (Fig. 15d), which resemble the pattern in the seasonal mean composite (Fig. 8c) but of substantially higher amplitude. This result again argues for the physical robustness of the seasonal mean composite pattern despite the limited statistical significance. A notable difference between EPC and EPN events particularly evident in Figs. 14 and 15 is the widespread Arctic cooling associated with EPC events (Fig. 14d, e) that contrasts the widespread Arctic warming of EPN events (Fig. 15e, f). We discuss this difference in further detail in the following section.

We illustrate the intraseasonal evolution of the precipitation anomalies in Fig. 16. Because the high-frequency precipitation variability is considerably noisier than Z300 or T2m, we calculated 11-day mean precipitation anomalies, and the lag is assigned to the central day of the 11-day interval. Although the precipitation composites are somewhat noisy, we see some of the features on these shorter timescales that are evident in seasonal composites (Fig. 8). In particular, EPC OLR events are considerably wetter over the Pacific Northwest as well as the central and eastern U.S. For example, at a lag of +15 days, EPC events are characterized by positive precipitation anomalies across all of the southern U.S. and northern Mexico (Fig. 16g), similar to the seasonal mean composite (Fig. 8b), but EPN events feature negative precipitation anomalies over southwestern and central North America (Fig. 16h).

4 Dynamical interpretations

This section provides discussion of some of the dynamical mechanisms that may contribute to the contrasts between the EPC and EPN teleconnection patterns, with a particular focus on differences in the North Pacific storm track and on Artic temperature anomalies.

4.1 Storm track variations

A notable difference between the EPC and EPN teleconnection patterns is an eastward shift of the composite EPC Z300 field relative to that of the EPN composite over the North Pacific region (Fig. 4). A plausible explanation for this difference is that an eastward extension of the tropical convection anomalies during EPC events results in an eastward extension of the Rossby wave source (Sardeshmukh and Hoskins 1988) and subsequent linear dispersion that gives rise to the North Pacific teleconnection pattern. As mentioned in the introduction, several studies have noted such a nonlinearity in ENSO teleconnections, and, consistent with our results, Hoerling et al. (2001) specifically single out the existence of the convective threshold as the source of a longitudinal shift in the North Pacific teleconnection pattern between El Niño and La Niña episodes and between weaker and stronger El Niño episodes.

Although linear dispersion from a diabatic heating source (e.g., Hoskins and Karoly 1981) provides the theoretical underpinning for the tropical excitation of

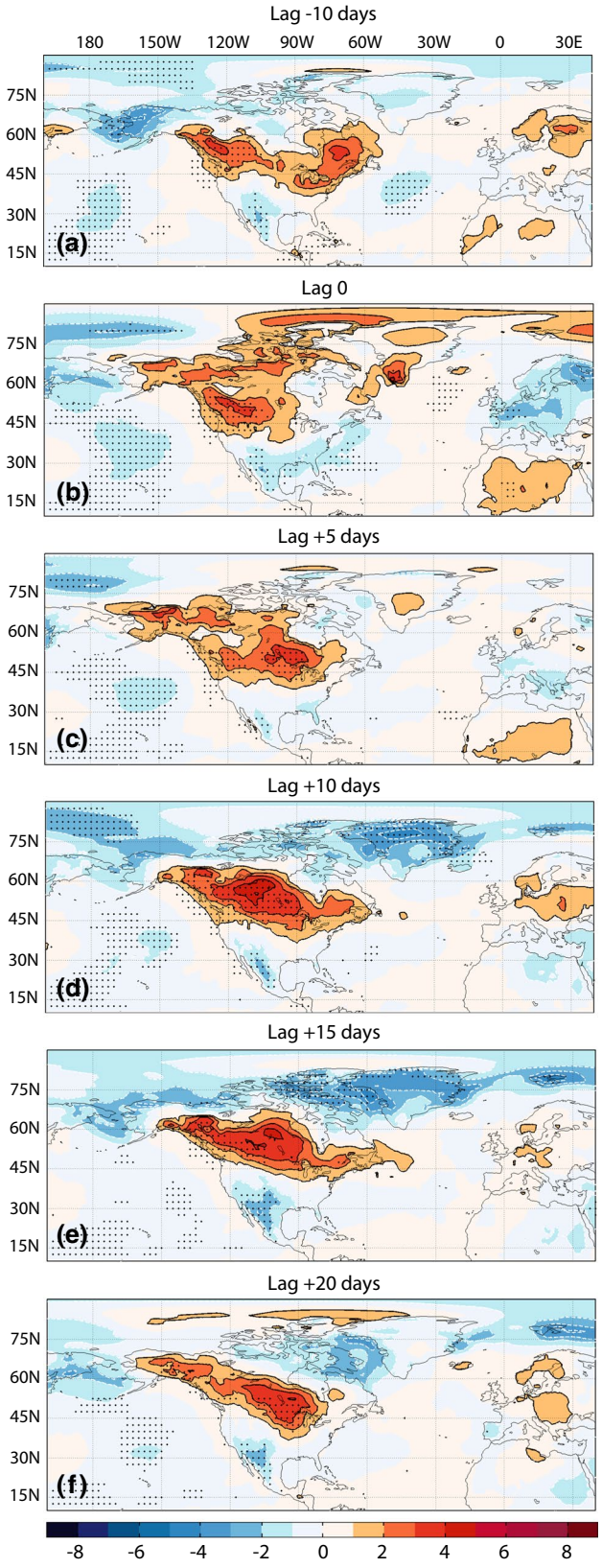

Fig. 14 As in Fig. 11 but for T2m anomalies (°C)

extratropical teleconnection patterns, numerous studies suggest that the changes in transient eddy activity also play a crucial role in the extratropical response to El Niño SST anomalies (Kok and Opsteegh 1985; Palmer and Mansfield 1986a; Held et al. 1989; Ting and Hoerling 1993; Hoerling and Ting 1994; Straus and Shukla 1997; Li et al. 2006; Harnik et al. 2010). These studies would seem to suggest that predictable variations in the El Niño teleconnections may relate strongly to differences in the storm tracks and the associated transient vorticity fluxes. Figure 17 illustrates the differences between EPC and EPN normalized storm track anomalies, as measured by anomalies of RMS bandpass-filtered 500 hPa streamfunction. EPC events feature enhanced synoptic eddy activity from the central to eastern North Pacific and into southern North America (Fig. 17a), indicating a southerly displacement and eastward extension of the storm track. Synoptic eddy activity is reduced in a northwest to southeast oriented band to the north of the enhanced storm track. The anomalies in synoptic eddy activity evident in Fig. 17a agree well with the canonical storm track response to El Niño reported in previous studies (Hoerling and Ting 1994; Straus and Shukla 1997; Harnik et al. 2010; Seager et al. 2010; Basu et al. 2013; Grise et al. 2013).

The normalized storm track anomalies for EPN events (Fig. 17b) feature a similar though weaker pattern over much of the North Pacific, but the eastward extension of the storm track into North America is conspicuously absent. The greater zonal extension of the EPC storm track likely explains why EPC events are much wetter across southern North America (Fig. 8). The differences between EPC and EPN synoptic eddy activity closely mirror the differences in the upper tropospheric zonal wind (Fig. 17c), a link that is consistent with several previous studies (Lau 1988; Straus and Shukla 1997; Seager et al. 2010; Grise et al. 2013).

A plausible hypothesis that emerges from Fig. 17 is that the eastward extension of tropical diabatic heating present in EPC events but absent in EPN events allows the subtropical jet to extend much farther eastward from its climatological position and serve as a more effective waveguide that directs synoptic eddies directly into southern North America. Through a series of idealized linear model experiments, Hoerling and Ting (1994) show that an eastward displacement of tropical heating into the equatorial eastern Pacific results in an upper level anticyclone and by continuity the subtropical jet that also shifts to the eastern Pacific. This change in basic state alters the refraction of transient eddies, allowing them to propagate more readily along the enhanced waveguide (Harnik et al. 2010; Seager et al. 2010). There likely is strong feedback between the

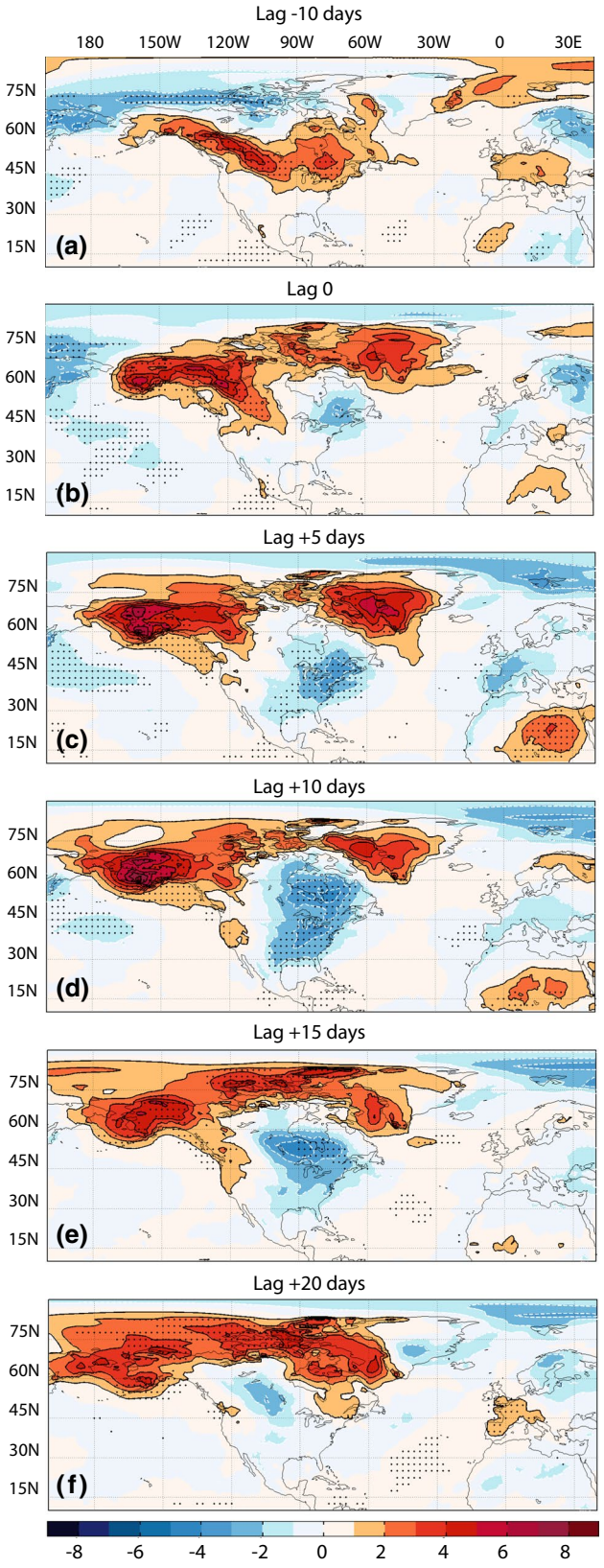

Fig. 15 As in Fig. 11 but for T2m anomalies (°C) and intraseasonal EPN OLR events

transient eddies and mean flow, and so disentangling the interactions between the tropically forced stationary wave and midlatitude transient eddies requires analysis of greater depth presented here. As a starting point, however, we can conclude that the difference in longitudinal extent of the tropical convective heating anomalies between EPC and EPN events likely results in differences in the teleconnection patterns due, at least in part, to the differences in the storm track and its interaction with the tropically forced Rossby wave.

4.2 Constructive and destructive interference with climatological stationary eddies

EPC and EPN El Niño composite impacts are notably distinct over the Arctic, where EPC (EPN) events are associated with Arctic cooling (warming) (Figs. 8, 14, 15). This distinction appears to be consistent with the so-called Tropically Excited Arctic warMing (TEAM) mechanism, whereby zonally localized tropical convection results in wintertime high-latitude warming but more zonally diffuse convective heating results in wintertime high-latitude cooling (Lee et al. 2011a, b; Lee 2012, 2014). The high-latitude warming by convection anomalies confined to the Indo-western Pacific warm pool region occurs through the excitation of poleward propagating Rossby waves and the resulting polar warming by wave dynamics and enhanced downward infrared radiation. This theory relates to constructive and destructive interference with the climatological stationary wave, as the zonally localized climatological warm pool convection gives rise, in part, to the climatological stationary wave that transports moist static energy poleward in the winter. Therefore, the enhancement (reduction) of the east–west contrast in tropical convection through localized warm pool convection anomalies, as we see for EPN (EPC) El Niño events (Figs. 3, 9), tend to force a Rossby wave that constructively (destructively) interferes with the stationary wave forced by the climatological warm pool convection, thereby increasing the poleward transport of moist static energy. The TEAM mechanism has support from idealized experiments with general circulation models (Lee et al. 2011a; Yoo et al. 2012b) and from analyses of observations (Lee et al. 2011b; Lee 2012; Yoo et al. 2012a), including impacts on Arctic sea ice (Park et al. 2015; Goss et al. 2016).

To determine whether the composite EPC and EPN streamfunction anomaly differences are consistent with the TEAM mechanism arguments presented above, we show in Fig. 18 normalized composites of 300 hPa eddy (i.e., the zonally asymmetric) streamfunction, the climatological 300 hPa eddy streamfunction (i.e., the climatological stationary wave), normalized OLR composite anomalies,

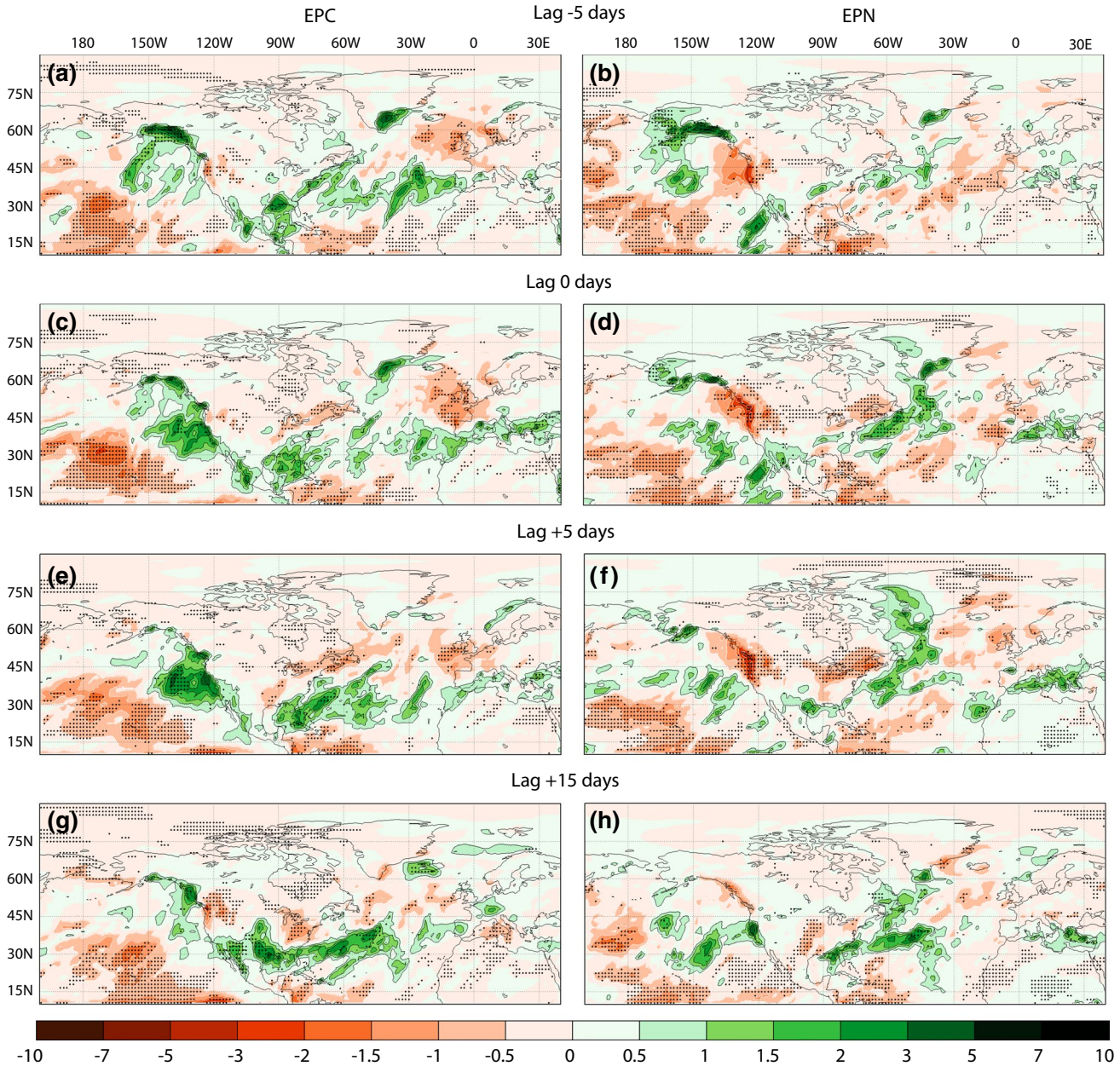

Fig. 16 Lagged composites of 11-day averaged precipitation anomalies (mm d^{-1}) for EPC (*left*) and EPN (*right*) OLR events. The central day of each composite corresponds with **a**, **b** lag −5, **c**, **d** lag 0, **e**, **f** lag +5, and **g**, **h** lag +15 days. *Stippling* indicates anomalies that are statistically significant at the 5 % level

and the tropical Indo-Pacific climatological OLR. For EPC (EPN) episodes, the OLR anomalies over the tropical Indo-Pacific region are generally out of phase (in phase) with the climatological OLR, indicating a reduction (enhancement) in the zonal gradient of tropical convection. Consistent with the TEAM mechanism, the 300 hPa streamfunction anomalies also are generally out of phase (in phase) with the climatological eddy streamfunction over the PNA region (Fig. 18a, b). The tendency for EPC (EPN) events to destructively (constructively) interfere with the climatological stationary eddy over the PNA region is particularly evident in the composite differences (Fig. 18c). The anomalously weak poleward propagating Rossby waves during EPC episodes implied by Fig. 18 also may help to explain the stronger subtropical jet (Fig. 17) because tropically excited Rossby waves can decelerate the subtropical jet (Lee 1999, 2012).

The results presented in Fig. 18 demonstrate consistency with the TEAM mechanism, providing a possible explanation for the Arctic cooling (warming) associated with

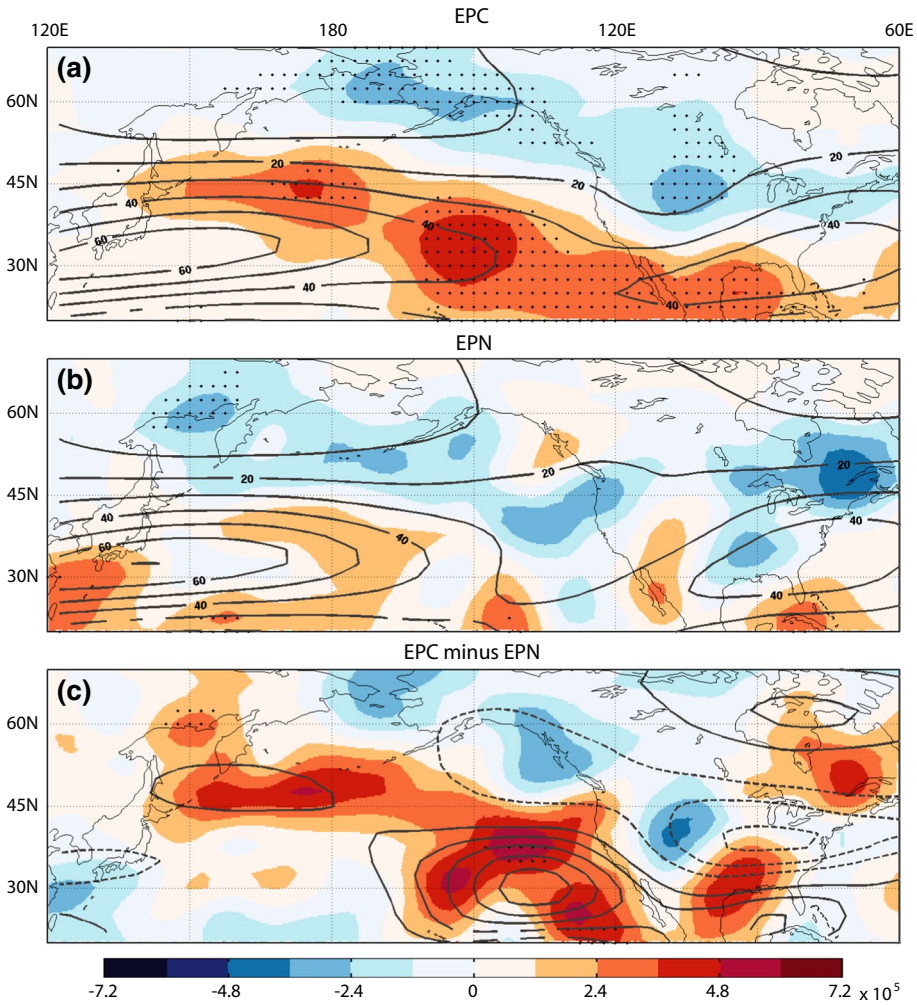

Fig. 17 December–March seasonal composites of RMS bandpass-filtered 500 hPa streamfunction anomalies normalized by the mean Niño 3.4 SST anomaly (*color shading* $m^2\ s^{-1}\ °C^{-1}$), and 200 hPa zonal wind (*grey contours* CI = 10 m s^{-1}) for **a** EPC and **b** EPN El Niño episodes. The composite difference is shown in **c**, where *solid* (*dashed*) contours indicate positive (negative) 200 hPa zonal wind differences (CI = 2 m s^{-1} and the zero contour is omitted). *Stippling* indicates statistically significant RMS bandpass-filtered streamfunction anomalies (**a**, **b**) or differences (**c**) at the 5 % level

EPC (EPN) El Niño episodes. Lee (2012) also invokes the TEAM mechanism to explain observed wintertime differences in high-latitude temperature anomalies between El Niño and La Niña episodes, as La Niña episodes, like with EPN El Niño, feature zonally localized tropical convection, enhanced poleward energy transport, and high-latitude warming. The arguments presented here, however, suggest that the optimal partitioning between high-latitude warming and cooling associated with ENSO may not fall along conventional distinctions between El Niño and La Niña; rather, the distinction between EPC and EPN El Niño may be more physically relevant because this partitioning marks the transition of anomalous tropical convection from climatologically favored regions to climatologically unfavorable regions.

Interestingly, Palmer and Mansfield (1986a) make a similar argument to describe the position of the subtropical anticyclonic anomalies in response to El Niño SST anomalies. Noting that Sverdrup vorticity balance in the Gill (1980) model cannot adequately describe the position of the anticyclones in response to the modeled tropical convective heating, they propose an alternative perspective: the El Niño SST anomalies reduce the zonal SST gradient, which reduces the zonally asymmetric component of vorticity, placing the anomalous anticyclones in the regions of climatological troughs. Figure 18 supports this perspective and extends the concept to the distinction between EPC and EPN teleconnection patterns throughout the entire PNA region.

5 Discussion

In this study, we provide evidence that the boreal winter teleconnections associated with EPC and EPN El Niño are fundamentally distinct in some regions, especially over North America and the Arctic. Outside of the PNA region, including the North Atlantic, Europe, and North Africa, the evidence of significant climate impacts from El Niño is more limited from the small sample sizes considered in this study, but there is some suggestion that the more remote impacts are more pronounced for EPN than

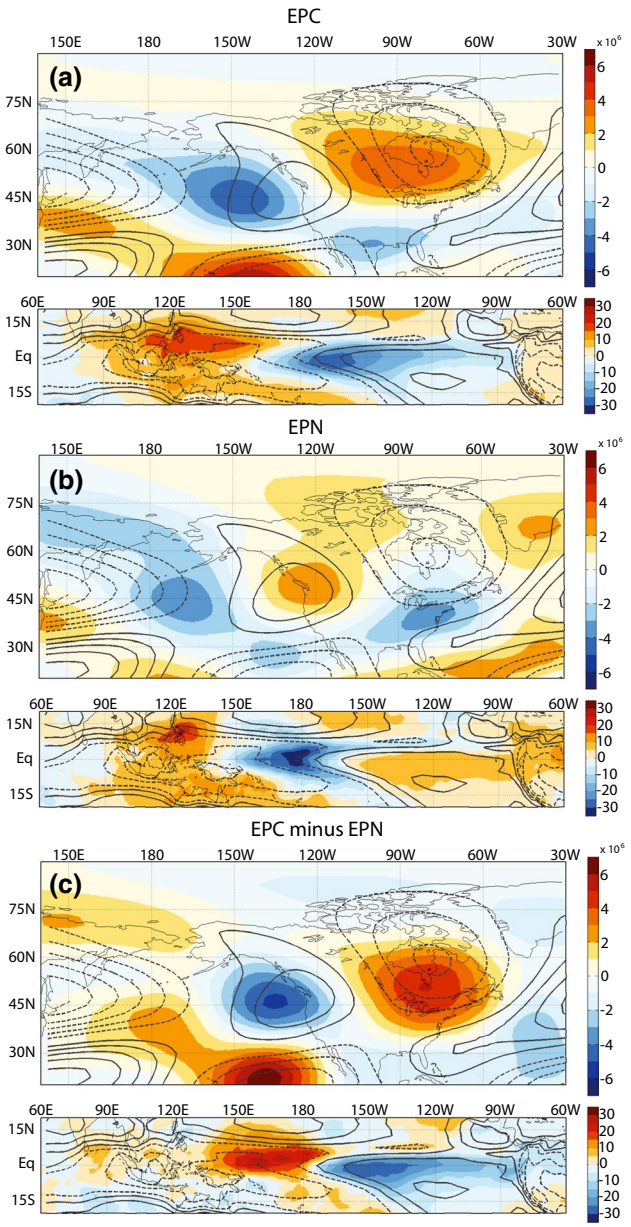

Fig. 18 December–March seasonal composites of (*top panels*) 300 hPa eddy (i.e., zonally asymmetric) streamfunction normalized by the mean Niño 3.4 SST anomaly (*color shading* m^2 s^{-1} $°C^{-1}$) with the climatological eddy streamfunction (*contours*), where *solid* (*dashed*) *grey contours* indicate positive (negative) values (CI = 4×10^6 m^2 s^{-1}, and the zero contour is omitted). *Bottom panels* show the normalized composites of OLR anomalies (*color shading* W m^{-2}) and climatological OLR (*grey contours*, CI = 10 W m^{-2}), where *solid contours* indicate OLR values of 250 W m^{-2} and greater, i.e., convectively inactive regions. Composites are calculated for **a** EPC and **b** EPN El Niño episodes, and the differences are shown in **c**

for EPC events (e.g., Figs. 4 and 8). The sources of these more remote El Niño impacts are subject to significant debate, but one hypothesis with substantial recent support involves stratospheric-tropospheric coupling (Brönnimann et al. 2004; Manzini et al. 2006; Taguchi and Hartmann 2006; Garfinkel and Hartmann 2008; Cagnazzo and Manzini 2009; Ineson and Scaife 2009; Fletcher and Kushner 2011, 2013; Butler et al. 2014; Sung et al. 2014). Recent work suggests that significant North Atlantic-European region impacts of El Niño may depend on the occurrence of sudden stratospheric warmings (SSWs), and so the absence of a SSW may preclude El Niño-related seasonal prediction in this sector (Butler et al. 2014; Domeisen et al. 2015). As with the TEAM mechanism, the basic principle relates to linear interference with the climatological stationary eddy (Garfinkel et al. 2010; Fletcher and Kushner 2011, 2013), as stationary eddies of large horizontal scale that transport heat poleward during the Northern Hemisphere winter propagate vertically. Tropically forced Rossby waves of low zonal wavenumbers that constructively interfere with the climatological stationary eddy therefore enhance the planetary wave driving in the stratosphere and weaken the stratospheric polar vortex. Through wave-mean flow interaction, this weakened vortex tends to propagate downward into the troposphere, manifesting as circulation anomalies that project onto the negative phase of the AO with substantial climate impacts over the North Atlantic and Eurasia. It is increasingly recognized that such linear interference is associated with El Niño episodes (Garfinkel and Hartmann 2008; Fletcher and Kushner 2011), although the relationship between stratospheric wave driving and ENSO is complex (e.g., Butler and Polvani 2011). The arguments presented in the previous section, however, suggest that the stratospheric-tropospheric interaction may vary between EPC and EPN episodes, with EPC (EPN) exhibiting a tendency to destructively (constructively) interfere with the climatological stationary eddy and possibly reducing (enhancing) the stratospheric planetary wave driving. Garfinkel and Hartmann (2008) note that of the teleconnection patterns associated with El Niño, the PNA is associated with a weakening of the polar vortex, but the TNH is not. Consistent with the speculation above, the EPN composite more closely resembles the PNA, whereas the EPC composite more closely resembles the TNH (Fig. 4). Livezey and Mo (1987) also documented a tendency for stronger El Niño episodes to project more strongly onto the TNH, a tendency not exhibited by the PNA. Garfinkel and Hartmann (2008, 2010) provide evidence through observational analysis and modeling experiments that the El Niño teleconnection pattern distinctions are most strongly related to the phase of the QBO, but an alternative possibility is that PNA/TNH distinction depends more on the pattern of tropical convection, as shown in this study.

Goss et al. (2016) provide indirect support for this linear interference hypothesis. They define a Northern Hemisphere stationary wave index to identify conditions associated with constructive and destructive interference with

the wintertime climatological stationary wave. They find that suppressed warm pool convection, like what occurs during EPC El Niño episodes, is associated with destructive interference, cooling of the Arctic, a strengthening of the stratospheric polar vortex, and an increase of the AO index. The occurrence of constructive interference, which features opposite effects, also bears strong similarity to the EPN El Niño effects except that the enhanced warm pool convection preceding constructive interference identified by Goss et al. (2016) is centered about 30°–40° west of the enhanced EPN El Niño convection (Fig. 9). There is some evidence, however, that counters the hypothesis that we propose. Modeling studies that impose idealized tropical SST anomalies in either the central or eastern tropical Pacific produce similar extratropical responses, particularly with respect to a weakening stratospheric polar vortex (Garfinkel et al. 2013; Hegyi et al. 2014). These results suggest that constructive interference may occur for both EPC and EPN El Niño. Given these conflicting lines of evidence, the possible distinctions in stratospheric-tropospheric interaction between EPC and EPN El Niño require additional careful study, particularly in light of the small sample sizes and several confounding factors like volcanic eruptions and the phase of the QBO. Such a study is reserved for future work.

The differences between the more regionally confined and the broader, more annual climate impacts also could have purely tropospheric origins. Through the use of climate model experiments with idealized SST forcing, Li et al. (2006) demonstrate that wintertime tropical Pacific convective heating anomalies confined to the west Pacific, between ~140 and 180°E, tend to force a hemispheric, negative AO-like circulation response, whereas heating anomalies confined to the east Pacific tend to produce a more regional, arching teleconnection pattern over the PNA region. Moreover, diagnoses with a linear dynamical model suggest that these differences relate strongly to the position of the transient forcing anomalies relative to the jet, with forcing within the jet core resulting in the broader, more annular response, and forcing outside the jet core resulting in a more regionally confined response. These findings suggest that the different longitudes of tropical heating between EPC and EPN events and the resulting differences in the anomalies of transient eddy activity may play an important role in the difference between a regional versus a more hemispheric atmospheric circulation response. Another possibility is that the more remote, predictable climate impacts outside of the PNA region relate to SST anomalies outside of the tropical Pacific (Mathieu et al. 2004), a hypothesis not examined in this study. This discussion highlights that recent studies raise a considerable number of plausible hypotheses but the physical mechanisms responsible for predictable variations in the EPC and EPN teleconnection patterns require further study.

In this study we only consider the boreal winter impacts, the season when both ENSO and its teleconnections tend to be strongest. However, it is likely that the EPC and EPN teleconnection pattern differences extend beyond boreal winter, given the long timescales of ocean variability and the memory imparted by the land surface (e.g., Schubert

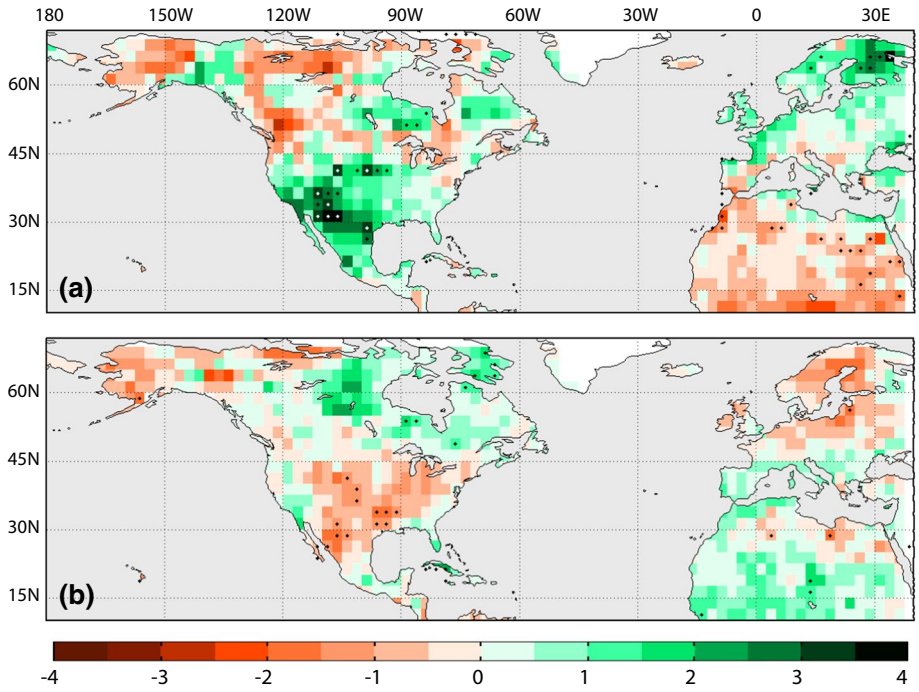

Fig. 19 June–August composite PDSI anomalies, normalized by the preceding mean December–March Niño 3.4 SST anomaly, for **a** EPC and **b** EPN El Niño episodes. *Green* (*brown*) shading indicates pluvial (drought) conditions. *Stippling* indicates composite anomalies that are statistically significant at the 5 % level based on a two-side Student's *t* test

et al. 2004). Regarding this latter source of potential predictability, the stark contrasts in precipitation composites between EPC and EPN El Niño (Fig. 8) suggest that distinct patterns of soil moisture anomalies may carry into subsequent seasons and, through feedbacks with the atmosphere, manifest as distinct tendencies for summertime droughts and pluvials. To support this speculation, Fig. 19 presents normalized composites of June–August PDSI for EPC and EPN El Niño episodes, again defined by equatorial eastern Pacific SST anomalies in the preceding December–March. The June–August PDSI composites largely reflect the wintertime precipitation anomalies over the contiguous U.S. and Mexico, whereby the wetter EPC events are associated with pluvial conditions over much of the western U.S. and northern Mexico (Fig. 19a), but the drier EPN events are associated with drought conditions over many of the same areas (Fig. 19b). The EPC and EPN PDSI composite anomalies actually are of opposite sign over a large fraction of the domain, including Europe and North Africa, although the statistical significance is limited. These preliminary findings suggest that the seasonal variations of the teleconnection differences deserve further scrutiny, with land–atmosphere interaction likely playing an increasingly important role during the warm season.

6 Summary

In this study, we argue along similar lines as in Chiodi and Harrison (2013, 2015) that the most potentially predictable variations of boreal winter El Niño teleconnection patterns relate to the distinction between convective (EPC) and non-convective (EPN) eastern Pacific events. A key distinction between this study and Chiodi and Harrison (2013, 2015) is that we argue that the partitioning between these two types of El Niño is a strong function of the eastern Pacific and tropical mean SSTs, as this partitioning relates to the nonlinear relationship between deep convection and SST in the eastern Pacific (Hoerling et al. 1997, 2001). For the period of overlap, the EPC/EPN partitioning by the RSST criterion agrees with the OLR/non-OLR El Niño partitioning except that Chiodi and Harrison (2013, 2015) classify the 2009/2010 event as non-OLR, whereas we classify the event as a marginal EPC event. Such differences in classification for borderline cases may be expected.

Establishing the link between SST and convective/non-convective eastern Pacific El Niño offers several potential advantages. First, it allows us to extend the analysis prior to the satellite era, increasing sample sizes and strengthening the robustness of the conclusions. Second, the SST link offers potentially enhanced usefulness for seasonal forecasts, as eastern Pacific SSTs are forecastable for lead times of at least several months—without the SST link, the potential forecasting benefits require a diagnosis of OLR anomalies in the initial conditions, reducing the lead times for which such a partitioning may be useful. Third, the framework provided here may be useful for understanding projected changes in El Niño teleconnection patterns. Although focus on this third point is reserved for a future study, the perspective offered here suggests that changes in the eastern Pacific RSST distribution, occurring through changes in the tropical Pacific mean state, ENSO variance, or a combination of the two, would change the proportion of EPC and EPN Niño episodes, thereby changing the mean El Niño teleconnection pattern.

Chiodi and Harrison (2015) also partition La Niña into OLR and non-OLR events based on the sum of strongly positive OLR days over a region of the western tropical Pacific (5°S–5°N, 150°E–180°). It is not clear how the concepts described in this study may apply to La Niña because the nonlinearity of deep convection with respect to SST applies to climatological SSTs below but near the convective threshold in the eastern Pacific and not to the climatologically warmer SSTs in the warm pool region. Therefore, any possible extension of the SST/OLR relationships to La Niña likely would need to invoke additional information about the SST evolution during La Niña that is distinct from the relationships described here.

In agreement with the results of Chiodi and Harrison (2013, 2015) for non-OLR El Niño, many of the composite EPN climate impacts are not statistically significant on seasonal timescales, which limits the conclusions that can be drawn from the analysis of seasonal composites alone. However, we argue that the EPN teleconnection patterns are, in fact, physically robust on subseasonal timescales when the signal-to-noise ratio sometimes is much higher than in the seasonal mean composite. For EPN events identified by subseasonal OLR anomalies, the extratropical composite anomalies are substantially stronger, statistically significant, and similar in structure as in the seasonal mean composites. These findings indicate that EPN events may have strong midlatitude impacts on intraseasonal timescales (~1–3 weeks) when the EPN pattern of tropical convection is active. Recently, a simple statistical model based on the combined influence of the MJO and ENSO sometimes yielded skillful wintertime temperature forecasts out to lead times of 4 weeks (Johnson et al. 2014), but that study did not account for possible variations in El Niño teleconnection patterns. The work presented here suggests that both EPC and EPN El Niño may provide sources of enhanced predictability at lead times of 2–4 weeks, but the expected impacts are quite distinct.

The physical mechanisms responsible for the differences between EPC and EPN teleconnection patterns require additional study, but perhaps the simplest explanation, following lines of reasoning in Palmer and Mansfield (1986a)

and Lee et al. (2011a), relates to constructive and destructive interference with the climatological stationary eddies: EPC (EPN) events weaken (strengthen) the zonal gradient of tropical Pacific convection, thereby exciting teleconnection patterns that tend to be out of phase (in phase) with the climatological stationary eddy over the PNA sector. Additional work is needed to understand the mechanisms of remote impacts outside of the PNA sector and in other seasons. The use of the RSST criterion to define EPC and EPN El Niño is based on the assumption that tropical tropospheric temperatures closely follow the tropical mean SST. Although we believe that the validity of this assumption is reasonable enough for the purposes of this study, recent work suggests that there may be substantial deviation from this tendency, particularly on interdecadal timescales (Flannaghan et al. 2014; Fueglistaler et al. 2015). Therefore, there may be room to refine the convective eastern Pacific criterion, perhaps through the incorporation of precipitation-weighted SST instead of the tropical mean SST, but such refinements would come at the cost of added complexity.

Acknowledgments We are grateful for stimulating discussions with Dr. Steven Feldstein, Dr. Sukyoung Lee, and Ms. Michelle L'Heureux, which enhanced this work. We also thank Dr. Andrew Wittenberg, Dr. Xiaosong Yang, and two anonymous reviewers for constructive comments that resulted in significant improvements of the manuscript. NCJ was supported by NOAA's Climate Program Office, which includes a grant from the Modeling, Analysis, Predictions, and Projections program, award number NA14OAR4310189. YK was supported by the Ministry of Education, Culture, Sports, Science and Technology (MEXT) of Japan through Grant-in-Aid for Young Scientists 15H05466 and by the Japanese Ministry of Environment through the Environment Research and Technology Development Fund 2-1503. NCEP–NCAR reanalysis and FACTS climate model simulation data are provided by the NOAA/OAR/ESRL PSD, Boulder, Colorado, USA, from their Web site at http://www.esrl.noaa.gov/psd.

References

Ashok K, Behera SK, Rao SA, Weng H, Yamagata T (2007) El Niño Modoki and its possible teleconnection. J Geophys Res 112:C11007. doi:10.1029/2006JC003798

Back L, Bretherton CS (2009) A simple model of climatological rainfall and vertical motion patterns over tropical oceans. J Clim 22:6477–6497. doi:10.1175/2009JCLI2393.1

Barnston AG, Chelliah M, Goldenberg SB (1997) Documentation of a highly ENSO-related SST region in the equatorial Pacific. Atmos Ocean 35:367–383. doi:10.1080/07055900.1997.9649597

Barsugli JJ, Sardeshmukh PD (2002) Global atmospheric sensitivity to tropical SST anomalies throughout the Indo-Pacific basin. J Clim 15:3427–3442. doi:10.1175/1520-0442(2002)015<3427:GASTTS>2.0.CO;2

Basu S, Zhang X, Polyakov I, Bhatt US (2013) North American winter-spring storms: modeling investigation on tropical Pacific sea surface temperature impacts. Geophys Res Lett 40:5228–5233. doi:10.1002/grl.50990

Brönnimann S (2007) Impact of El Niño-Southern Oscillation on European climate. Rev Geophys 45:RG3003. doi:10.1029/2006RG000199

Brönnimann S, Luterbacher J, Staehelin J, Svendby TM, Hansen G, Svenøe T (2004) Extreme climate of the global troposphere and stratosphere in 1940–42 related to El Niño. Nature 431:971–974. doi:10.1038/nature02982

Butler AH, Polvani LM (2011) El Niño, La Niña, and stratospheric sudden warmings: a reevaluation in light of the observational record. Geophys Res Lett 38:L13807. doi:10.1029/2011GL048084

Butler AH, Polvani LM, Deser C (2014) Separating the stratospheric and tropospheric pathways of El Niño-Southern Oscillation teleconnections. Environ Res Lett 9:024014. doi:10.1088/1748-9326/9/2/024014

Cagnazzo C, Manzini E (2009) Impact of the stratosphere on the winter tropospheric teleconnections between ENSO and the North Atlantic and European region. J Clim 22:1223–1238. doi:10.1175/2008JCLI2549.1

Capotondi A, Wittenberg AT, Newman M, Di Lorenzo E, Yu J-Y, Braconnot P, Cole J, Dewitte B, Giese B, Guilyardi E, Jin F-F, Karnauskas K, Kirtman B, Lee T, Schneider N, Xue Y, Yeh SW (2015) Understanding ENSO diversity. Bull Am Meteorol Soc. doi:10.1175/BAMS-D-13-00117.1

Chiodi AM, Harrison DE (2013) El Niño impacts on seasonal U.S. atmospheric circulation, temperature, and precipitation anomalies: the OLR-event perspective. J Clim 26:822–837. doi:10.1175/JCLI-D-12-00097.1

Chiodi AM, Harrison DE (2015) Global seasonal precipitation anomalies robustly associated with El Niño and La Niña events—an OLR perspective. J Clim 28:6133–6159. doi:10.1175/JCLI-D-14-00387.1

Dai A, Trenberth KE, Qian T (2004) A global data set of Palmer Drought Severity Index for 1870–2002: relationship with soil moisture and effects of surface warming. J Hydrol 5:1117–1130. doi:10.1175/JHM-386.1

Dee DP et al (2011) The ERA-Interim reanalysis: configuration and performance of the data assimilation system. Q J R Meteorol Soc 137:553–597. doi:10.1002/qj.828

DeWeaver E, Nigam S (2002) Linearity in ENSO's atmospheric response. J Clim 15:2447–2461. doi:10.1175/1520-0442(2002)015<2446:LIESAR>2.0.CO;2

Domeisen DIV, Butler AH, Fröhlich K, Bittner M, Müller WA, Baehr J (2015) Seasonal predictability over Europe arising from El Niño and stratospheric variability in the MPI-ESM seasonal prediction system. J Clim 28:256–271. doi:10.1175/JCLI-D-14-00207.1

Fan Y, Van den Dool H (2008) A global monthly land surface air temperature analysis for 1948-present. J Geophys Res 113:D01103. doi:10.1029/2007JD008470

Feldstein SB (2000) The timescale, power spectra, and climate noise properties of teleconnection patterns. J Clim 13:4430–4440. doi:10.1175/1520-0442(2000)013<4430:TTPSAC>2.0.CO;2

Feldstein SB (2002) Fundamental mechanisms of the growth and decay of the PNA teleconnection pattern. Q J R Meteorol Soc 128:775–796. doi:10.1256/0035900021643683

Flannaghan TJ, Fueglistaler S, Held IM, Po-Chedley S, Wyman B, Zhao M (2014) Tropical temperature trends in atmospheric general circulation model simulations and the impact of uncertainties in observed SSTs. J Geophys Res 119:13327–13337. doi:10.1002/2014JD022365

Fletcher CG, Kushner PJ (2011) The role of linear interference in the annular mode response to tropical SST forcing. J Clim 24:778–794. doi:10.1175/2010JCLI3735.1

Fletcher CG, Kushner PJ (2013) Linear interference and the northern annular mode response to tropical SST forcing: sensitivity

to model configuration. J Geophys Res 118:4267–4279. doi:10.1002/jgrd.50385
Fraedrich K, Müller K (1992) Climate anomalies in Europe associated with ENSO extremes. Int J Climatol 12:25–31. doi:10.1002/joc.3370120104
Frauen C, Dommenget D, Tyrrell N, Rezny M, Wales S (2014) Analysis of the nonlinearity of El Niño-Southern Oscillation teleconnections. J Clim 27:6225–6244. doi:10.1175/JCLI-D-13-00757.1
Fueglistaler S, Radley S, Held IM (2015) The distribution of precipitation and the spread in tropical upper tropospheric temperature trends in CMIP5/AMIP simulations. Geophys Res Lett 42:6000–6007. doi:10.1002/2015GL064966
Gadgil S, Joseph V, Joshi NV (1984) Ocean-atmosphere coupling over monsoon regions. Nature 312:141–143. doi:10.1038/312141a0
Garfinkel CI, Hartmann DL (2008) Different ENSO teleconnections and their effects on the stratospheric polar vortex. J Geophys Res 113:D18114. doi:10.1029/2008JD009920
Garfinkel CI, Hartmann DL (2010) Influence of the quasi-biennial oscillation on the North Pacific and El Niño teleconnections. J Geophys Res 115:D20116. doi:10.1029/2010JD014181
Garfinkel CI, Hartmann DL, Sassi F (2010) Tropospheric precursors of anomalous Northern Hemisphere stratospheric polar vortices. J Clim 23:3282–3299. doi:10.1175/2010JCLI3010.1
Garfinkel CI, Hurwitz MM, Waugh DW, Butler AH (2013) Are the teleconnections of Central Pacific and Eastern Pacific El Niño distinct in boreal wintertime? Clim Dyn 41:1835–1852. doi:10.1007/s00382-012-1570-2
Gershunov A, Barnett TP (1998) Interdecadal modulation of ENSO teleconnections. Bull Am Meteorol Soc 17:2715–2725. doi:10.1175/1520-0477(1998)079<2715:IMOET>2.0.CO;2
Giese BS, Ray S (2011) El Niño variability in simple ocean data assimilation (SODA), 1871–2008. J Geophys Res 116:C02024. doi:10.1029/2010JC006695
Gill AE (1980) Some simple solutions for heat-induced tropical circulation. Q J R Meteorol Soc 106:447–462. doi:10.1002/qj.49710644905
Goss M, Feldstein SB, Lee S (2016) Stationary wave interference, and its relation to tropical convection and Arctic warming. J Clim. doi:10.1175/JCLI-D-15-0267.1
Graf H-F, Zanchettin D (2012) Central Pacific El Niño, the "subtropical bridge", and Eurasian climate. J Geophys Res 117:D01102. doi:10.1029/2011JD016493
Grise KM, Son S-W, Gyakum JR (2013) Intraseasonal and interannual variability in the North American storm tracks and its relationship to equatorial Pacific variability. Mon Weather Rev 141:3610–3625. doi:10.1175/MWR-D-12-00322.1
Halpert MS, Ropelewski CF (1992) Surface temperature patterns associated with the Southern Oscillation. J Clim 5:577–593. doi:10.1175/1520-0442(1992)005<0577:STPAWT>2.0.CO;2
Hannachi A (2001) Toward a nonlinear identification of the atmospheric response to ENSO. J Clim 14:2138–2149. doi:10.1175/1520-0442(2001)014<2138:TANIOT>2.0.CO;2
Harnik N, Seager R, Naik N, Cane M, Ting M (2010) The role of linear wave refraction in the transient eddy-mean flow response to tropical Pacific SST anomalies. Q J Meteorol Soc 136:2132–2146. doi:10.1002/qj.688
Hegyi BM, Deng Y, Black RX, Zhou R (2014) Initial transient response of the winter polar stratospheric vortex to idealized equatorial Pacific sea surface temperature anomalies in the NCAR WACCM. J Clim 27:2699–2713. doi:10.1175/JCLI-D-13-00289.1
Held IM, Lyons SW, Nigam S (1989) Transients and the extratropical response to El Niño. J Atmos Sci 46:163–174. doi:10.1175/1520-0469(1989)046<0163:TATERT>2.0.CO;2
Hoerling MP, Kumar A (1997) Why do North American climate anomalies differ from one El Niño event to another? Geophys Res Lett 24:1059–1062. doi:10.1029/97GL00918
Hoerling MP, Ting M (1994) Organization of extratropical transients during El Niño. J Clim 7:745–766. doi:10.1175/1520-0442(1994)007<0745:OOETDE>2.0.CO;2
Hoerling MP, Kumar A, Zhong M (1997) El Niño, La Niña, and the nonlinearity of their teleconnections. J Clim 10:1769–1786. doi:10.1175/1520-0442(1997)010<1769:ENOLNA>2.0.CO;2
Hoerling MP, Kumar A, Xu T (2001) Robustness of the nonlinear climate response to ENSO's extreme phases. J Clim 14:1277–1293. doi:10.1175/1520-0442(2001)014<1277:ROTNCR>2.0.CO;2
Hoerling M, Kumar A, Dole R, Nielsen-Gammon JW, Eischeid J, Perlwitz J, Quan X-W, Zhang T, Pegion P, Chen M (2013) Anatomy of an extreme event. J Clim 26:2811–2832. doi:10.1175/JCLI-D-12-00270.1
Horel JD, Wallace JM (1981) Planetary-scale atmospheric phenomena associated with the Southern Oscillation. Mon Weather Rev 109:813–829. doi:10.1175/1520-0493(1981)109<0813:PSAPAW>2.0.CO;2
Hoskins BJ, Karoly DJ (1981) The steady linear response of a spherical atmosphere to thermal and orographic forcing. J Atmos Sci 38:1179–1196. doi:10.1175/1520-0469(1981)038<1179:TSLROA>2.0.CO;2
Hu ZZ, Kumar A, Jha B, Wang W, Huang B, Huang B (2012) An analysis of warm pool and cold tongue El Niños: air–sea coupling processes, global influences, and recent trends. Clim Dyn 38:2017–2035. doi:10.1007/s00382-011-1224-9
Ineson S, Scaife AA (2009) The role of the stratosphere in the European climate response to El Niño. Nat Geosci 2:32–36. doi:10.1038/ngeo381
Jin F-F, Hoskins BJ (1995) The direct response to tropical heating in a baroclinic atmosphere. J Atmos Sci 52:307–319. doi:10.1175/1520-0469(1995)052<0307:TDRTTH>2.0.CO;2
Johnson NC (2013) How many ENSO flavors can we distinguish? J Clim 26:4816–4827. doi:10.1175/JCLI-D-12-00649.1
Johnson NC, Feldstein SB (2010) The continuum of North Pacific sea level pressure patterns: intraseasonal, interannual, and interdecadal variability. J Clim 23:851–867. doi:10.1175/2009JCLI3099.1
Johnson NC, Xie S-P (2010) Changes in the sea surface temperature threshold for tropical convection. Nat Geosci 3:842–845. doi:10.1038/ngeo1008
Johnson NC, Collins DC, Feldstein SB, L'Heureux ML, Riddle EE (2014) Skillful wintertime North American temperature forecasts out to 4 weeks based on the state of ENSO and the MJO. Weather Forecast 29:23–38. doi:10.1175/WAF-D-13-00102.1
Kalnay E et al (1996) The NCEP/NCAR 40-year reanalysis project. Bull Am Meteorol Soc 77:437–471. doi:10.1175/1520-0477(1996)077<0437:TNYRP>2.0.CO;2
Kao H-Y, Yu J-Y (2009) Contrasting eastern-Pacific and central-Pacific types of ENSO. J Clim 22:615–632. doi:10.1175/2008JCLI2309.1
Kiladis GN, Diaz HF (1989) Global climatic anomalies associated with extremes in the Southern Oscillation. J Clim 2:1069–1090. doi:10.1175/1520-0442(1989)002<1069:GCAAWE>2.0.CO;2
Kok CJ, Opsteegh JD (1985) Possible causes of anomalies in seasonal mean circulation patterns during the 1982–83 El Niño event. J Atmos Sci 42:677–694. doi:10.1175/1520-0469(1985)042<0677:PCOAIS>2.0.CO;2
Kug J-S, Jin F-F, An S-I (2009) Two types of El Niño events: Cold tongue El Niño and warm pool El Niño. J Clim 22:1499–1515. doi:10.1175/2008JCLI2624.1
Kumar A, Hoerling MP (1995) Prospects and limitations of seasonal atmospheric GCM predictions. Bull Am Meteorol Soc

76:335–345. doi:10.1175/1520-0477(1995)076<0335:PALOSA>2.0.CO;2

Kumar A, Hoerling MP (1997) Interpretation and implications of observed inter-El Niño variability. J Clim 10:83–91. doi:10.1175/1520-0442(1997)010<0083:IAIOTO>2.0.CO;2

Kumar A, Zhang Q, Peng P, Jha B (2005) SST-forced atmospheric variability in an atmospheric general circulation model. J Clim 18:3953–3967. doi:10.1175/JCLI3483.1

L'Heureux ML, Tippett MK, Barnston AG (2015) Characterizing ENSO coupled variability and its impact on North American seasonal precipitation and temperature. J Clim 28:4231–4245. doi:10.1175/JCLI-D-14-00508.1

Larkin NK, Harrison DE (2005) On the definition of El Niño and associated seasonal average U.S. weather anomalies. Geophys Res Lett 32:L13705. doi:10.1029/2005GL022738

Lau N-C (1988) Variability of the observed midlatitude storm tracks in relation to low-frequency changes in circulation patterns. J Atmos Sci 45:2718–2743. doi:10.1175/1520-0469(1988)045<2718:VOTOMS>2.0.CO;2

Lee S (1999) Why are the climatological zonal mean winds easterly in the equatorial upper troposphere? J Atmos Sci 56:1353–1363. doi:10.1175/1520-0469(1999)056<1353:WATCZW>2.0.CO;2

Lee S (2012) Testing of the tropically excited Arctic warming mechanism (TEAM) with traditional El Niño and La Niña. J Clim 25:4015–4022. doi:10.1175/JCLI-D-12-00055.1

Lee S (2014) A theory for polar amplification from a general circulation perspective. Asia Pac J Atmos Sci 50:31–43. doi:10.1007/s13143-014-0024-7

Lee S, Feldstein SB, Pollard D, White TS (2011a) Do planetary wave dynamics explain equable climates? J Clim 24:2391–2404. doi:10.1175/2011JCLI3825.1

Lee S, Gong T, Johnson N, Feldstein SB, Pollard D (2011b) On the possible link between tropical convection and the Northern Hemisphere Arctic surface air temperature change between 1958 and 2001. J Clim 24:4350–4367. doi:10.1175/2011JCLI4003.1

Li S, Hoerling MP, Peng S, Weickmann KM (2006) The annular response to tropical Pacific SST forcing. J Clim 19:1802–1819. doi:10.1175/JCLI3668.1

Liebmann B, Smith CA (1996) Description of a complete (interpolated) outgoing longwave radiation dataset. Bull Am Meteorol Soc 77:1275–1277

Livezey RE, Mo KC (1987) Tropical-extratropical teleconnections during the Northern Hemisphere winter. Part II: relationships between monthly mean Northern Hemisphere circulation patterns and proxies for tropical convection. Mon Weather Rev 115:3115–3132. doi:10.1175/1520-0493(1987)115<3115:TETDTN>2.0.CO;2

Madden RA, Julian PR (1971) Detection of a 40–50 day oscillation in the zonal wind in the tropical Pacific. J Atmos Sci 28:702–708. doi:10.1175/1520-0469(1971)028<0702:DOADOI>2.0.CO;2

Manzini E, Giorgetta MA, Esch M, Kornblueh L, Roeckner E (2006) The influence of sea surface temperatures on the northern winter stratosphere: ensemble simulations with the MAECHAM5 Model. J Clim 19:3863–3881. doi:10.1175/JCLI3826.1

Mathieu P-P, Sutton RT, Dong B, Collins M (2004) Predictability of winter climate over the North Atlantic European region during ENSO events. J Clim 17:1953–1974. doi:10.1175/1520-0442(2004)017<1953:POWCOT>2.0.CO;2

Mo KC (2010) Interdecadal modulation of the impact of ENSO on precipitation and temperature over the United States. J Clim 23:3639–3656. doi:10.1175/2010JCLI3553.1

Mo KC, Livezey RE (1986) Tropical–extratropical geopotential height teleconnections during the Northern Hemisphere winter. Mon Weather Rev 114:2488–2515. doi:10.1175/1520-0493(1986)114<2488:TEGHTD>2.0.CO;2

Molod A, Takacs L, Suarez M, Bacmeister J, Somg I, Eichmann A (2012) The GEOS-5 atmospheric general circulation model: mean climate and development from MERRA to Fortuna. NASA Technical report series on global modeling and data assimilation, NASA TM2012-104606, 117 pp

Neale RB, Richter JH, Conley AJ, Park S, Lauritzen PH, Gettelman A, Williamson DL, Rasch PJ, Vavrus SJ, Taylor MA, Collins WD, Zhang M, Lin S-J (2010) Description of the NCAR community atmosphere model (CAM 4.0). NCAR technical note NCAR/TN-XXX+STR, National Center for Atmospheric Research, 212 pp

Neale RB et al (2012) Description of the NCAR community atmosphere model (CAM 5.0). NCAR technical note NCAR/TN-486+STR, National Center for Atmospheric Research, 274 pp

Palmer TN, Mansfield DA (1986a) A study of wintertime circulation anomalies during past El Niño events using a high resolution general circulation model. I: influence of model climatology. Q J R Meteorol Soc 112:613–638. doi:10.1002/qj.49711247304

Palmer TN, Mansfield DA (1986b) A study of wintertime circulation anomalies during past El Niño events using a high resolution general circulation model. II: variability of the seasonal mean response. Q J R Meteorol Soc 112:639–660. doi:10.1002/qj.49711247305

Park H-S, Lee S, Son S-W, Feldstein SB, Kosaka Y (2015) The impact of poleward moisture and sensible heat flux on Arctic winter sea ice variability. J Clim. doi:10.1175/JCLI-D-15-0074.1

Peng P, Kumar A (2005) A large ensemble analysis of the influence of tropical SSTs on seasonal atmospheric variability. J Clim 18:1068–1085. doi:10.1175/JCLI-3314.1

Ray S, Giese BS (2012) Historical changes in El Niño and La Niña characteristics in an ocean reanalysis. J Geophys Res 117:C11007. doi:10.1029/2012JC008031

Roeckner E, Bäuml G, Bonaventura L, Brokopf R, Esch M, Giorgetta M, Hagemann S, Kirchner, Kornblueh L, Manzini E, Rhodin A, Schlese U, Schulzweida U, Tompkins A (2003) The atmospheric general circulation model ECHAM5. Part I: model description. Max Planck Institute for Meteorology, 127 pp

Ropelewski CF, Halpert MS (1987) Global and regional scale precipitation patterns associated with the El Niño/Southern Oscillation. Mon Weather Rev 115:1606–1626. doi:10.1175/1520-0493(1987)115<1606:GARSPP>2.0.CO;2

Saha S et al (2014) The NCEP climate forecast system version 2. J Clim 27:2185–2208. doi:10.1175/JCLI-D-12-00823.1

Sardeshmukh PD, Hoskins BJ (1988) The generation of global rotational flow by steady idealized tropical divergence. J Atmos Sci 45:1228–1251. doi:10.1175/1520-0469%281988%29045<1228%3ATGOGRF>2.0.CO%3B2

Sardeshmukh PD, Compo GP, Penland C (2000) Changes of probability associated with El Niño. J Clim 13:4268–4286. doi:10.1175/1520-0442(2000)013<4268:COPAWE>2.0.CO;2

Schneider U, Becker A, Finger P, Meyer-Christoffer A, Rudolph B, Ziese M (2011) GPCC full data reanalysis version 6.0 at 1.0: monthly land-surface precipitation from rain-gauges built on GTS-based and historic data. doi:10.5676/DWD_GPCC/FD_M_V6_100

Schneider U, Becker A, Finger P, Meyer-Christoffer A, Ziese M, Rudolph B (2013) GPCC's new land surface precipitation climatology based on quality-controlled in situ data and its role in quantifying the global water cycle. Theor Appl Climatol 115:15–40. doi:10.1007/s00704-013-0860-x

Schubert SD, Suarez MJ, Pegion PJ, Koster RD, Bacmeister JT (2004) Causes of long-term drought in the U.S. Great Plains. J Clim 17:485–503. doi:10.1175/1520-0442(2004)017<0485:COLDIT>2.0.CO;2

Schubert SD, Wang H, Koster RD, Suarez MJ, Groisman PY (2014) Northern Eurasian heat waves and droughts. J Clim 27:3169–3207. doi:10.1175/JCLI-D-13-00360.1

Screen JA, Simmonds I (2010) The central role of diminishing sea ice in recent Arctic temperature amplification. Nature 464:1334–1337. doi:10.1038/nature09051

Seager R, Naik N, Ting M, Cane MA, Harnik N, Kushnir Y (2010) Adjustment of the atmospheric circulation to tropical Pacific SST anomalies: variability of transient eddy propagation in the Pacific-North America sector. Q J R Meteorol Soc 136:277–296. doi:10.1002/qj.588

Smith TM, Reynolds RW, Peterson TC, Lawrimore J (2008) Improvements to NOAA's historical merged land-ocean surface temperature analysis (1880–2006). J Clim 21:2283–2296. doi:10.1175/2007JCLI2100.1

Sobel AH, Nilsson J, Polvani LM (2001) The weak temperature gradient approximation and balanced tropical moisture waves. J Atmos Sci 58:3650–3665. doi:10.1175/1520-0469(2001)058<3650:TWTGAA>2.0.CO;2

Sobel AH, Held IM, Bretherton CS (2002) The ENSO signal in tropical tropospheric temperature. J Clim 15:2702–2706. doi:10.1175/1520-0442(2002)015<2702:TESITT>2.0.CO;2

Straus DM, Shukla J (1997) Variations of midlatitude transient dynamics associated with ENSO. J Atmos Sci 54:777–790. doi:10.1175/1520-0469(1997)054<0777:VOMTDA>2.0.CO;2

Sung M-K, Kim B-M, An S-I (2014) Altered atmospheric responses to eastern Pacific and central Pacific El Niños over the North Atlantic region due to stratospheric interference. Clim Dyn 42:159–170. doi:10.1007/s00382-012-1661-0

Taguchi M, Hartmann DL (2006) Increased occurrence of stratospheric sudden warmings during El Niño as simulated by WACCM. J Clim 19:324–332. doi:10.1175/JCLI3655.1

Takahashi K, Montecinos A, Goubanova K, Dewitte B (2011) ENSO regimes: reinterpreting the canonical and Modoki El Niño. Geophys Res Lett 38:L10704. doi:10.1029/2011GL047364

The GFDL Global Atmospheric Model Development Team (2005) The new GFDL global atmosphere and land model AM2–LM2: evaluation with prescribed SST simulations. J Clim 17:4641–4673. doi:10.1175/JCLI-3223.1

Ting M, Hoerling MP (1993) Dynamics of stationary wave anomalies during the 1986/87 El Niño. Clim Dyn 9:147–164. doi:10.1007/BF00209751

Toniazzo T, Scaife A (2006) The influence of ENSO on winter North Atlantic climate. Geophys Res Lett 33:L24704. doi:10.1029/2006GL027881

Trenberth KE (1997) The definition of El Niño. Bull Am Meteorol Soc 78:2771–2777. doi:10.1175/1520-0477(1997)078<2771:TDOENO>2.0.CO;2

Trenberth KE, Caron JM (2000) The Southern Oscillation revisited: sea level pressures, surface temperatures, and precipitation. J Clim 13:4358–4365. doi:10.1175/1520-0442(2000)013<4358:TSORSL>2.0.CO;2

Trenberth KE, Smith L (2009) Variations in the three-dimensional structure of the atmospheric circulation with different flavors of El Niño. J Clim 22:2978–2991. doi:10.1175/2008JCLI2691.1

Trenberth KE, Branstator GW, Karoly D, Kumar A, Lau N-G, Ropelewski C (1998) Progress during TOGA in understanding and modeling global teleconnections associated with tropical sea surface temperatures. J Geophys Res 103:14291–14324. doi:10.1029/97JC01444

Trenbeth KE, Stepaniak DP (2001) Indices of El Niño evolution. J Clim 14:1697–1701. doi:10.1175/1520-0442(2001)014<1697:LIOENO>2.0.CO;2

Weng H, Ashok K, Behera SK, Rao SA, Yamagata T (2007) Impacts of recent El Niño Modoki on dry/wet conditions in the Pacific Rim during boreal summer. Clim Dyn 29:113–129. doi:10.1007/s00382-007-0234-0

Wheeler MC, Hendon HH (2004) An all-season real-time multivariate MJO index: development of an index for monitoring and prediction. Mon Weather Rev 132:1917–1932. doi:10.1175/1520-0493(2004)132<1917:AARMMI>2.0.CO;2

Xie S-P, Deser C, Vecchi GA, Ma J, Teng H, Wittenberg AT (2010) Global warming pattern formation: sea surface temperature and rainfall. J Clim 23:966–986. doi:10.1175/2009JCLI3329.1

Xue Y, Smith TM, Reynolds RW (2003) Interdecadal changes of 30-yr SST normals during 1871–2000. J Clim 16:1601–1612. doi:10.1175/1520-0442%282003%29016<1601%3AICOYSN>2.0.CO%3B2

Yoo C, Lee S, Feldstein SB (2012a) Mechanisms of extratropical surface air temperature change in response to the Madden–Julian Oscillation. J Clim 25:5777–5790. doi:10.1175/JCLI-D-11-00566.1

Yoo C, Lee S, Feldstein SB (2012b) Arctic response to an MJO-like tropical heating in an idealized GCM. J Atmos Sci 69:2379–2393. doi:10.1175/JAS-D-11-0261.1

Yu J-Y, Kao H-Y (2007) Decadal changes of ENSO persistence barrier in SST and ocean heat content indices: 1958–2001. J Geophys Res 112:D13106. doi:10.1029/2006JD007654

Yu J-Y, Zou Y (2013) The enhanced drying effect of Central-Pacific El Niño on US winter. Environ Res Lett 8:014019. doi:10.1088/1748-9326/8/1/014019

Yu J-Y, Zou Y, Kim ST, Lee T (2012) The changing impact of El Niño on US winter temperatures. Geophys Res Lett 39:L15702. doi:10.1029/2012GL052483